

# Oxygen abundances in metal-poor subgiants as determined from [O I], O I and OH lines\*

A.E. García Pérez<sup>1, \*\*</sup>, M. Asplund<sup>2</sup>, F. Primas<sup>3</sup>, P.E. Nissen<sup>4</sup>, and B. Gustafsson<sup>1</sup>

<sup>1</sup> Department of Astronomy and Space Physics, Box 515 SE-751 20 Uppsala, Sweden

<sup>2</sup> Mt. Stromlo Observatory, Cotter Rd., Weston, ACT 2611, Australia

<sup>3</sup> European Southern Observatory, Karl-Schwarzschild Str. 2, D-85748 Garching b. München, Germany

<sup>4</sup> Department of Physics and Astronomy, University of Århus, DK-8000 Århus C, Denmark

Received: soon; accepted: quite soon

**Abstract.** The debate on the oxygen abundances of metal-poor stars has its origin in contradictory results obtained using different abundance indicators. To achieve a better understanding of the problem we have acquired high quality spectra with the Ultraviolet and Visual Echelle Spectrograph at VLT, with a signal-to-noise of the order of 100 in the near ultraviolet and 500 in the optical and near infrared wavelength range. Three different oxygen abundance indicators, OH ultraviolet lines around 310.0 nm, the [O I] line at 630.03 nm and the O I lines at 777.1-5 nm were observed in the spectra of 13 metal-poor subgiants with  $-3.0 \leq [\text{Fe}/\text{H}] \leq -1.5$ . Oxygen abundances were obtained from the analysis of these indicators which was carried out assuming local thermodynamic equilibrium and plane-parallel model atmospheres. Abundances derived from O I were corrected for departures from local thermodynamic equilibrium. Stellar parameters were computed using  $T_{\text{eff}}$ -vs-color calibrations based on the infrared flux method and Balmer line profiles, Hipparcos parallaxes and Fe II lines. [O/Fe] values derived from the forbidden line at 630.03 nm are consistent with an oxygen/iron ratio that varies linearly with [Fe/H] as  $[\text{O}/\text{Fe}] = -0.09(\pm 0.08)[\text{Fe}/\text{H}] + 0.36(\pm 0.15)$ . Values based on the O I triplet are on average  $0.19 \pm 0.22$  dex (s.d.) higher than the values based on the forbidden line while the agreement between OH ultraviolet lines and the forbidden line is much better with a mean difference of the order of  $-0.09 \pm 0.25$  dex (s.d.). In general, our results follow the same trend as previously published results with the exception of the ones based on OH ultraviolet lines. In that case our results lie below the values which gave rise to the oxygen abundance debate for metal-poor stars.

**Key words.** line: formation – stars: abundances – stars: atmospheres – stars: population II – Galaxy: evolution

## 1. Introduction

Oxygen plays a major role in astrophysics through its high cosmic abundance. It is predominantly produced and ejected back into the interstellar medium in connection with core-collapse supernovae (SNe II). By comparing oxygen abundances in stars of different ages with those of iron, which is produced both in SNe II and in thermo-nuclear supernovae of white dwarfs (SNe Ia), one can probe the star formation rate history and initial mass function of a galaxy as well as the physics of supernovae (e.g. Tinsley 1980; Wheeler et al. 1989). Due to the longer time-scale of

Fe production in SNe Ia, one can expect an oxygen over-abundance relative to iron at low metallicity:  $[\text{O}/\text{Fe}] > 0^1$ .

While such an oxygen over-abundance in metal-poor stars has long been known to exist (Conti et al. 1967), the exact amount is still contested with no unanimous agreement apparently in sight. Broadly speaking the derived [O/Fe] values depend on which oxygen diagnostic is employed in the analysis and what type of stars is observed. There are four different types of spectral transitions which have been utilised for this purpose: the forbidden [O I] 630.0 and 636.3 nm lines, high excitation O I lines, in particular the O I 777.1-5 nm triplet, OH A-X electronic lines in the ultraviolet (UV) and OH vibration-rotation lines in the infrared (IR). The O I and OH lines have mainly been used in metal-poor turn-off stars ( $T_{\text{eff}} \gtrsim 6000$  K) while the O abundances in halo giants ( $T_{\text{eff}} \lesssim 5000$  K) are typically based on the [O I] lines.

Send offprint requests to: aegp@astro.uu.se

\* Based on observations collected at the European Southern Observatory, Chile (ESO No. 68.D-0546)

\*\* Student visitor at the European Southern Observatory, Munich, Germany

<sup>1</sup> The abundance ratios are defined by the customary  $[\text{X}/\text{Fe}] = \log(N_{\text{X}}/N_{\text{Fe}})_{*} - \log(N_{\text{X}}/N_{\text{Fe}})_{\odot}$ .

The [O I] lines suggest a quasi-plateau at  $[O/Fe] \sim +0.5$  for  $[Fe/H] \leq -1$  (e.g. Barbuy 1988; Sneden et al. 1991; Nissen et al. 2002). This has traditionally been advocated as the correct metallicity trend, in particular since the first studies based on the OH lines in the UV gave consistent results (Bessell et al. 1984, 1991; Nissen et al. 1994). More recently, the OH lines in the IR have also been studied in a few stars with a similar result, at least when restricting to weak, higher excitation OH lines (Balachandran et al. 2001; Meléndez et al. 2001). Systematically higher [O/Fe] values are normally derived when using the O I triplet (e.g. Abia & Rebolo 1989; Israelian et al. 1998, 2001; Boesgaard et al. 1999; Carretta et al. 2000; Nissen et al. 2002; Fulbright & Johnson 2003), sometimes interpreted as a steady linear increase in [O/Fe] towards lower [Fe/H]. The O I triplet results have often been blamed on departures from local thermodynamic equilibrium (LTE), effects of inhomogeneities and/or an erroneous  $T_{\text{eff}}$ -scale in order to reconcile them with the [O I] results. The issue of oxygen abundances in halo stars received much renewed attention following the surprising results of Israelian et al. (1998, 2001) and Boesgaard et al. (1999) who found a near linear trend in [O/Fe] with a significant slope of about  $-0.4$  towards lower metallicity from OH lines in the UV in turn-off stars and a couple of subgiants.

All of the above-mentioned oxygen diagnostics have their advantages and disadvantages. The O I triplet is susceptible to non-LTE effects (NLTE) (Kiselman 2001, and references therein) and is, due to the high excitation potential, quite sensitive to the adopted  $T_{\text{eff}}$ . The [O I] line is immune to departures from LTE but is essentially undetectable in turn-off stars with  $[Fe/H] \lesssim -2$  due to its weakness. The OH lines are very sensitive to the temperature structure in the stellar atmosphere. Given the much lower temperatures encountered in the optically thin layers in 3D hydrodynamical model atmospheres compared with classical 1D hydrostatic models for metal-poor stars (Asplund et al. 1999), large downward abundance corrections have been flagged for the OH lines in turn-off stars. The [O I] lines are also affected by such temperature inhomogeneities but to a lesser degree than the OH lines (Nissen et al. 2002), while the NLTE line formation of the O I lines can be suspected to be dependent on the 3D atmospheric structure as well (Kiselman & Nordlund 1995; Asplund & García Pérez 2001; Asplund et al. 2004). Additional complications and confusion stem from the differences and uncertainties in the adopted  $T_{\text{eff}}$  and  $\log g$ , the use of Fe I or Fe II lines to derive [Fe/H], possible missing continuous opacities in the UV (Balachandran & Bell 1998; Bell et al. 2001) and which solar oxygen abundance the stellar values are referenced to. Given the recent large downward revision of the solar O abundance to  $\log \epsilon_{\text{O}} \sim 8.7$  (Allende Prieto et al. 2001; Asplund et al. 2004), this difference of about 0.2 dex compared with the previously advocated value (Anders & Grevesse 1989) will directly translate to a corresponding *increase* in [O/Fe].

Considering all these remaining uncertainties it is perhaps not surprising that no consensus has as yet been

achieved in terms of the behaviour of [O/Fe] with [Fe/H]. It is noteworthy that significant differences between the different oxygen indicators only reveal themselves at low metallicities ( $[Fe/H] \lesssim -2$ ), which is observationally very challenging due to the weakness of some of the spectral features. The fact that the different oxygen diagnostics are normally used in different types of stars constitutes a major problem in this regard. The only metal-poor stars for which it is possible to employ molecular as well as forbidden and permitted atomic lines are subgiants but also then exceptionally high-quality spectra are required. Until now, only two halo subgiants (HD 140283 and BD+23°3130, both with  $[Fe/H] \sim -2.4$ ) have been analysed with [O I], O I and OH UV lines (Israelian et al. 1998, 2001; Fulbright & Kraft 1999; Cayrel et al. 2001; Balachandran et al. 2001; Nissen et al. 2002), with somewhat ambiguous results. Our best hope to finally resolve this important outstanding problem is offered by halo subgiants. In the present article we present such a study based on very high-quality UV and optical spectra for a sample of 13 subgiants with  $-3.0 \leq [Fe/H] \leq -1.5$ .

## 2. Observations

We identified a sample of halo subgiants based on Hipparcos parallaxes and/or Strömgren photometry with metallicity  $-3.0 \leq [Fe/H] \leq -1.5$ . From this sample, high-quality spectra were acquired for 13 subgiants using the UVES (Dekker et al. 2000) at ESO's Very Large Telescope (VLT) 8m Kueyen telescope. The observations were carried out in service mode between October 2000 and March 2001. The use of the dichroic capability of UVES enabled simultaneous observations of the UV and optical region to cover the three most important oxygen abundance diagnostics: OH A-X lines around 310.0 nm, the [O I] 630.03 nm line and the O I 777.1-5 nm lines. Due to the relatively low effective temperature of the targets, the observing times were largely determined by the requirement to obtain reasonable signal-to-noise ( $S/N$ ) in the UV (resulting in  $S/N \sim 100-150$  at 310.0 nm). This enabled the total exposure time to be split between two optical settings to cover both the forbidden and permitted O I lines and still achieve very high  $S/N$  ( $> 500$  in the centre of an echelle order at both 630 and 777 nm, although as will be described further below the O I triplet falls close to the edge of two orders in most cases resulting in typical values of  $S/N \sim 250$  at the triplet). We thus used two different dichroic settings for the red arm of the spectrograph (580 and 860 nm) together with the 346 nm setting for the blue arm. In total, the spectra covered 302.4-388.4 nm and 476.4-1061.0 nm, with near complete coverage in these regions. In all cases, at least three different exposures were obtained in each setting to allow efficient removal of cosmic rays.

For the blue arm, a projected slit-width of  $1.0''$  was used while for the red arm the width was  $0.7''$ . The resulting nominal spectral resolving powers associated with these slit-widths were 45 000 and 55 000, respectively, with

4 pixels per spectral resolution element. In order to gain  $S/N$  in the UV and because of oversampling, a 2x2 binning was used when reading out the EEV CCD without losing any spectral resolution.

As there are several telluric lines due to in particular  $H_2O$  and  $O_2$  around 630.03 nm, the [O I] line could be blended by telluric features depending on the radial velocity of the star and the particular date of the observations. We tried to avoid such problems by placing time constraints on when the observations should be carried out in service mode. For this purpose, we obtained radial velocity information of our targets from SIMBAD and computed the location of the stellar line in relation to the telluric lines for the relevant observing period. The procedure worked very well with one exception in which the radial velocity reported by SIMBAD turned out to be different from the actual value (given in Table 1) by about  $20 \text{ km s}^{-1}$ . As a result, our spectra of this star (CD  $-24^\circ$  1782) shows the [O I] 630.03 nm significantly distorted by telluric absorption, unfortunately rendering it useless for an abundance analysis.

The procedure followed in the data reduction was the classical one: subtraction of bias, definition of the echelle orders, division by the normalised flat-field, extraction of the orders, wavelength calibration and continuum normalization, all carried out within IRAF. The continuum was fitted using cubic spline functions. Due to the metal-poor nature of our targets, it was always relatively straightforward to identify wavelength regions without significant line contributions in the optical to make the continuum well defined. The UV region is more crowded even in metal-poor stars but it was still possible to find sufficiently many apparently clean continuum regions in the neighborhood of the OH lines. For the UV spectral region, the  $S/N$  was modest and hence the UVES pipeline reduction worked well, making a special data reduction unwarranted.

As mentioned above, care was taken when preparing for the observations in order to minimise the risk for blending of the [O I] line with telluric lines. Additional precautions in this regard were taken by obtaining spectra of rapidly rotating B stars during the same nights and at about the same airmass as the programme stars. In a few cases when the stellar [O I] line was partially blended by such telluric absorption, we relied on the IRAF task *telluric*, which worked well. The task optimises the fit between the telluric lines of the programme star and the B star by allowing a relative scaling in airmass and a shift in wavelength. The stars in our sample with partially blended [O I] lines are HD 4306, HD 26169, HD 45282, HD 126587, HD 128279 and HD 218857.

Observed stellar radial velocities for the stars were derived from the Doppler shifts of three Ca I (612.22, 616.22, 643.91 nm) and one Fe I (623.07 nm) lines. The resulting heliocentric velocities are given in Table 1.

### 3. Model atmospheres and stellar parameters

Before proceeding to determining element abundances for our sample, the stellar fundamental parameters must be estimated. The effective temperature ( $T_{\text{eff}}$ ), surface gravity ( $\log g$ ), metallicity ( $[Fe/H]$ ) and microturbulence ( $\xi_{\text{turb}}$ ) are the parameters needed to specify standard 1D model atmospheres. Such model atmospheres are used to calculate theoretical stellar spectra which can be compared with observed spectra directly, or indirectly by comparing observed and computed equivalent widths of spectral lines.

#### 3.1. Model atmospheres

The transport of radiation in the stellar atmospheres needs to be modelled in order to enable comparison with the observed spectra. For the purpose, we have calculated theoretical 1D LTE model atmospheres in hydrostatic equilibrium using the MARCS program (Gustafsson et al. 1975; Asplund et al. 1997) for the stellar parameters associated with the observed stellar sample. These models are based on up-to-date continuous opacities and include the effects of line-blanketing through opacity sampling. In the program, the convective energy flux is estimated using the mixing-length theory, assuming a mixing-length parameter  $\alpha = 1.5$ . The models have all been computed using a microturbulence  $\xi_{\text{turb}} = 1.0 \text{ km s}^{-1}$ . The adopted solar element abundances for the construction of the model atmospheres stem from Grevesse & Sauval (1998) with the exception of O which is taken from the 1D estimate of Nissen et al. (2002):  $\log \epsilon_{\text{O}} = 8.74$ . The chemical compositions of the models corresponding to our stellar sample are then scaled by the stellar metallicity, assuming that all the  $\alpha$ -elements (with carbon not included) were enhanced by 0.4 dex.

The solar oxygen and iron abundances used to estimate  $[O/Fe]$  and  $[Fe/H]$  were derived using a solar MARCS model atmosphere with the stellar parameters  $T_{\text{eff}} = 5780 \text{ K}$ ,  $\log g = 4.44$  [cgs] and  $[Fe/H] = 0.00$  and adopting a microturbulence  $\xi_{\text{turb}} = 1.15 \text{ km s}^{-1}$  for the spectral line formation calculations. The basic reason for our choice of a theoretical MARCS model to represent the solar atmosphere instead of a semiempirical one, such as the Holweger-Mueller model, was the ambition to make the analysis differential as far as possible, where systematic errors in models used for the Sun and the programme stars hopefully could cancel to a considerable extent.

#### 3.2. Reddening

The majority of stars in our sample are more distant than 200 pc according to their Hipparcos parallaxes. For these distances interstellar extinction could become important and the observed stellar magnitudes and stellar colours have to be corrected of reddening. Fortunately, most of the stars are found at high galactic latitudes where reddening in general is limited. Two different methods have been con-

**Table 1.** List of observed stars including coordinates,  $wby\beta$  photometry,  $(V - K)$  colour, Hipparcos parallaxes and the measured radial velocity from our observations

| Star        | $\alpha(2000)$<br>[hr:min:s] | $\delta(2000)$<br>[°:':"] | $V$<br>[mag] | $(b - y)$<br>[mag] | $m_1$<br>[mag] | $c_1$<br>[mag] | $\beta$<br>[mag] | $(V - K)$<br>[mag] | $\pi$<br>[mas] | $\sigma(\pi)$<br>[mas] | $v_r$<br>[km s <sup>-1</sup> ] |
|-------------|------------------------------|---------------------------|--------------|--------------------|----------------|----------------|------------------|--------------------|----------------|------------------------|--------------------------------|
| HD 4306     | 00:45:27.2                   | -09 : 32 : 39.8           | 9.035        | 0.518              | 0.052          | 0.348          | 2.529            | 2.212              | 4.81           | 1.40                   | -69.8                          |
| HD 26169    | 04:00:52.4                   | -75 : 36 : 11.5           | 8.797        | 0.523              | 0.051          | 0.328          | 2.521            | 2.163              | 2.83           | 0.79                   | -35.6                          |
| HD 27928    | 04:22:55.1                   | -37 : 15 : 49.2           | 9.554        | 0.506              | 0.067          | 0.295          | 2.523            | 2.106              | 2.36           | 1.16                   | 43.3                           |
| HD 45282    | 06:26:40.8                   | 03 : 25 : 29.8            | 8.028        | 0.451              | 0.108          | 0.277          | 2.544            | 1.939              | 7.34           | 0.96                   | 305.7                          |
| HD 108317   | 12:26:36.8                   | 05 : 18 : 09.0            | 8.036        | 0.447              | 0.055          | 0.291          | 2.548            | 1.883              | 4.53           | 1.06                   | 6.6                            |
| HD 126587   | 14:27:00.4                   | -22 : 14 : 39.0           | 9.119        | 0.602              | 0.042          | 0.460          | .....            | 2.451              | 1.40           | 1.44                   | 149.6                          |
| HD 128279   | 14:36:48.5                   | -29 : 06 : 46.6           | 8.039        | 0.467              | 0.055          | 0.262          | 2.545            | 1.974              | 5.96           | 1.32                   | -76.0                          |
| HD 200654   | 21:06:34.7                   | -49 : 57 : 50.3           | 9.097        | 0.460              | 0.027          | 0.271          | 2.534            | 1.943              | 3.20           | 1.25                   | -46.1                          |
| HD 218857   | 23:11:24.6                   | -16 : 15 : 04.0           | 8.967        | 0.506              | 0.076          | 0.371          | .....            | 2.094              | 3.51           | 1.42                   | -170.9                         |
| HD 274939   | 05:33:18.0                   | -47 : 56 : 13.8           | 9.435        | 0.494              | 0.128          | 0.300          | 2.526            | 2.136              | 2.88           | 1.06                   | 172.0                          |
| BD-01° 2582 | 11:53:37.3                   | -02 : 00 : 36.7           | 9.595        | 0.493              | 0.097          | 0.298          | .....            | 1.997              | 2.98           | 1.35                   | 0.8                            |
| CD-24° 1782 | 03:38:41.5                   | -24 : 02 : 50.3           | 9.934        | 0.466              | 0.040          | 0.287          | 2.526            | 1.975              | 4.42           | 1.75                   | 101.0                          |
| CD-30° 0298 | 00:58:43.9                   | -30 : 05 : 57.7           | 10.80        | 0.483              | 0.025          | 0.296          | .....            | 1.973              | 1.06           | 2.23                   | 27.2                           |

sidered for estimating reddening: the maps of infrared dust emission by Schlegel et al. (1998) and the models of visual interstellar extinction by Hakkila et al. (1997). In addition, the calibration of the interstellar doublet NaI lines at 589.0 and 589.6 nm by Munari & Zwitter (1997) have been taken into account in some cases for comparison purposes. Schlegel et al. (1998) used the COBE/DIRBE and IRAS/ISSA infrared maps of dust emission over the entire sky to estimate the dust column density. To proceed from the dust column density to reddening they used colours of elliptical galaxies. An important aspect of these maps is the possible presence of filamentary details. Hakkila et al. (1997) calculated reddenings based on published results of large-scale visual interstellar extinction. While the reddening estimates based on the model by Hakkila et al. depend on the assumed stellar distances, the estimates from the IR dust emission maps of Schlegel et al. give the reddening that an object will have if it would lie outside the dusty Galaxy.

The estimated reddening values  $E_{(B-V)}$  for both the Schlegel et al. and Hakkila et al. methods are given in Table 2 together with the galactic longitude and latitude. The values based on Schlegel et al. are almost always higher than those derived from Hakkila et al. In Fig. 1 the differences between the two methods are displayed against stellar distance and galactic latitude. There may be an indication that the greatest differences occur for low galactic latitudes. It is difficult to assess which values are more accurate. The uncertainties in the reddening given by Schlegel et al. are claimed to be of the order of 16%, Hakkila et al. estimate the errors to be about 0.07 mag. Indeed, the differences we have found could be interpreted as an indication of the uncertainty in the estimated reddening values. However, we believe that the Hakkila-based values may give a better description of the interstellar dust distribution in the solar neighborhood. We also note that the IR dust maps used by Schlegel et al. may be contaminated by infrared point sources that could not be properly

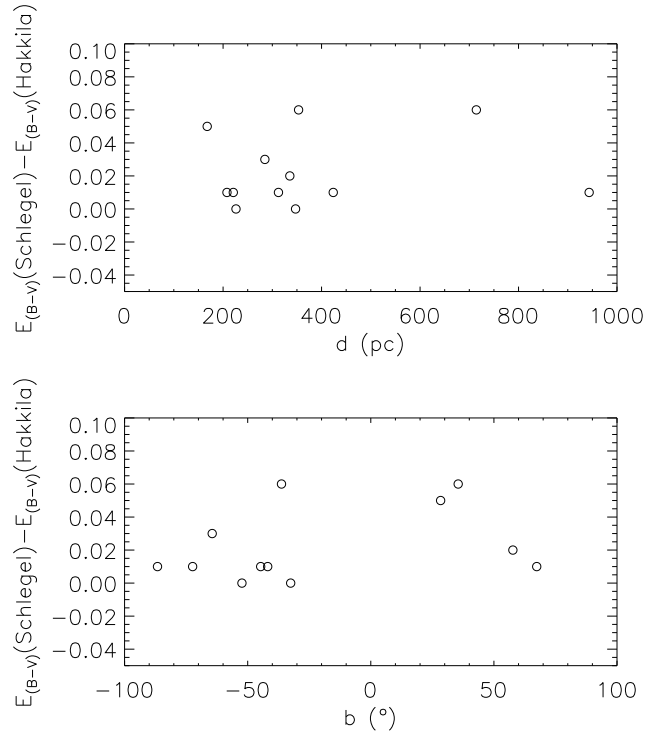


**Fig. 1.** Comparison of reddening estimates based on the two methods by Hakkila et al. (1997) and Schlegel et al. (1998). The differences are plotted versus the stellar distance in parsecs ( $d$ ) in the upper panel and versus the Galactic latitude of the star in degrees ( $b$ ) in the bottom panel. Note that HD 45282 is not shown in the figure as it would fall well outside the plot limits ( $\Delta E_{(B-V)} = 0.78$ ).

eliminated. One such example is HD 45282 for which the Schlegel et al. value is  $E_{(B-V)} = 0.82$ . HD 45282 is a relatively nearby star ( $d \sim 140$  pc) so the IR dust emission maps most probably overestimate the reddening, although we note that the star is located at low latitudes. As will be seen below, with  $E_{(B-V)} = 0.82$  the effective tempera-

**Table 2.** The galactic coordinates and reddenings determined using the methods of Hakkila et al. (1997) and Schlegel et al. (1998)

| Star        | $l$<br>[°] | $b$<br>[°] | $E_{(B-V)}$<br>[mag] | $E_{(B-V)}$<br>[mag] |
|-------------|------------|------------|----------------------|----------------------|
| HD 4306     | 118.057    | -72.359    | 0.03                 | 0.04                 |
| HD 26169    | 289.820    | -36.268    | 0.02                 | 0.08                 |
| HD 27928    | 239.682    | -44.720    | 0.02                 | 0.03                 |
| HD 274939   | 254.431    | -32.541    | 0.03                 | 0.03                 |
| HD 45282    | 207.050    | -3.930     | 0.04                 | (0.82)               |
| HD 108317   | 286.675    | 67.387     | 0.01                 | 0.02                 |
| HD 126587   | 330.345    | 35.489     | 0.04                 | 0.10                 |
| HD 128279   | 329.070    | 28.356     | 0.05                 | 0.10                 |
| HD 200654   | 348.821    | -41.873    | 0.02                 | 0.03                 |
| HD 218857   | 52.926     | -64.414    | 0.01                 | 0.04                 |
| BD-01° 2582 | 275.101    | 57.703     | 0.00                 | 0.02                 |
| CD-24° 1782 | 217.842    | -52.332    | 0.02                 | 0.02                 |
| CD-30° 0298 | 275.051    | -86.625    | 0.01                 | 0.02                 |

ture for this subgiant would be more than 8000 K, obviously an impossibly large value for a star, e.g. showing OH lines, which strengthens our belief that the Hakkila et al. method is to be preferred for our programme stars.

The equivalent widths of the interstellar NaI doublet at 589 nm can also provide an independent estimate of the reddening; our VLT-spectra covered this wavelength region as well. This has been tried for a few stars for comparison with the results of the other two methods. It is not always possible to make useful reddening estimates with this method due to blending with stellar lines or due to multiple interstellar components. To isolate the interstellar component of the lines, we performed spectrum synthesis using atomic data from the The Vienna Atomic Line Data Base (VALD) (Piskunov et al. 1995). As an example, HD 26169 shows a relatively strong main interstellar absorption as illustrated in Figure 2. According to Munari & Zwitter (1997) the equivalent width of the interstellar NaI D 589.0 nm absorption line of 15.0 pm corresponds to  $E_{(B-V)} = 0.05$ . This is in between the reddening estimates presented in Table 2 from the Schlegel et al. and Hakkila et al. models. The line in the case of HD 45282 is much weaker ( $\sim 2$  pm) which suggests a very low reddening, lower than 0.05. The interstellar contribution to the line will be even weaker if it turns out to be blended with a telluric line. Unfortunately, the interstellar NaI of the fast-rotator calibration star lies approximately at the same observer’s wavelength as the line of concern. Hence, it not possible to identify any telluric blend by just comparing the observed spectra of these two stars.

### 3.3. Effective temperature: photometry

The effective temperatures have been estimated using optical and IR broad-band and Strömgren photometry, in particular  $(V-K)$  and  $(b-y)$  colours. The  $V$  and  $uvby\beta$  photometry comes from Schuster & Nissen (1988) and pri-

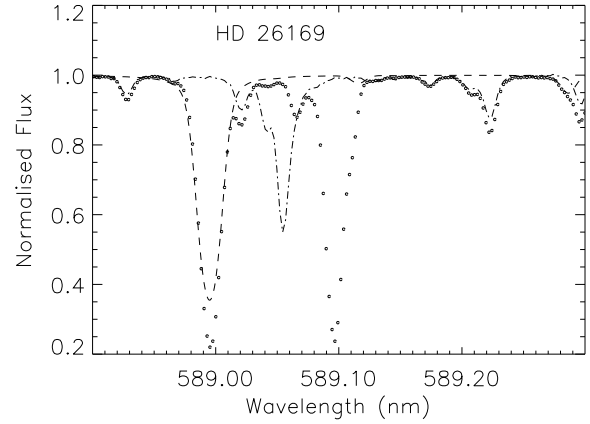


**Fig. 2.** The observed (open circles) and synthetic (dashed line) spectrum of HD 26169 around the NaI D 589.0 nm line. Also shown is the observed spectrum of the B star HR 1705 (dot-dashed line), to help identifying the telluric lines in the observed spectrum of HD 26169. The spectral feature around 589.1 nm is the interstellar absorption line.

vate communication, while the  $K$  magnitudes come from The Two Micron All Sky Survey (2MASS) database. The photometric data together with the parallaxes for the programme stars are given in Table 1. As described above, we have used the Hakkila et al. interstellar extinction maps to estimate reddenings, which have been applied to de-redden the stellar photometry. To convert the de-reddened  $(b-y)$  and  $(V-K)$  colours to  $T_{\text{eff}}$  estimates, we have used the calibrations by Alonso et al. (1999), which are based on the infrared flux method:

$$\theta_{(V-K)} = 0.5558 + 0.2105(V-K) + 0.001981(V-K)^2 - 0.009965(V-K)[Fe/H] + 0.01325[Fe/H] - 0.002726[Fe/H]^2 \quad (1)$$

$$\theta_{(b-y)} = 0.5815 + 0.7263(b-y) + 0.06856(b-y)^2 - 0.06832(b-y)[Fe/H] - 0.01062[Fe/H] - 0.01079[Fe/H]^2 \quad (2)$$

$$T_{\text{eff}} = 5040/\theta. \quad (3)$$

As the subgiants of the observed sample are ascending the red giant branch we have used the calibrations for giants rather than for dwarfs. We note, however, that the differences in temperature between the two calibrations are small. In our case, the dwarf calibration would have resulted in about 50 K lower values.

The agreement between  $T_{\text{eff}}(V-K)$  and  $T_{\text{eff}}(b-y)$  is quite good, as illustrated in Fig. 3. The mean difference is  $9.70 \pm 52$  K (s.d.) with a maximum difference of 108 K. There is no obvious trend in these differences with  $T_{\text{eff}}$ , although there may be a correlation with  $[Fe/H]$ . The latter conclusion, however, hinges entirely on the two least metal-poor stars with  $[Fe/H] \simeq -1.5$ . The mean of values

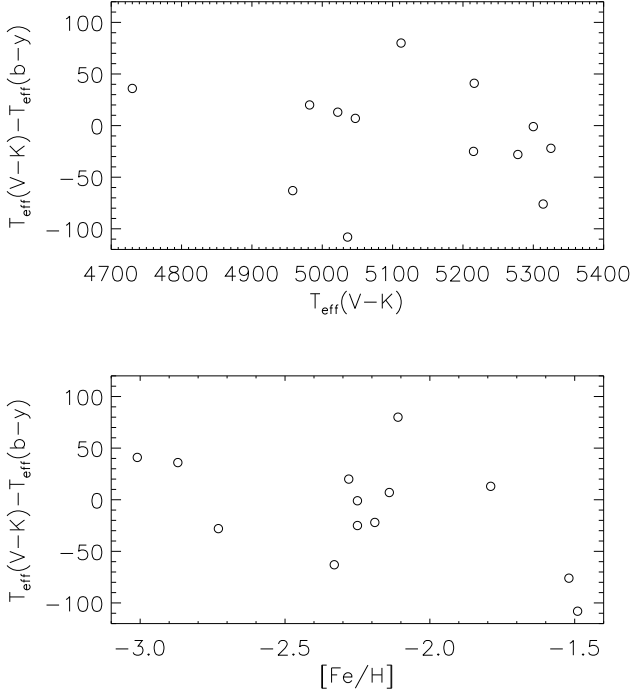


**Fig. 3.** Difference in  $T_{\text{eff}}$  when using the de-reddened  $(V - K)$  and  $(b - y)$  colours following Eq. 1 and Eq. 2, respectively. The temperature differences are shown in the top panel as a function of  $T_{\text{eff}}$  (determined from  $(V - K)$ ) and in the bottom panel versus  $[\text{Fe}/\text{H}]$ .

based on the de-reddened  $(b - y)_0$  and  $(V - K)_0$  colours were adopted as the final stellar effective temperature. The resulting photometric  $T_{\text{eff}}$  values are listed in Table 3 together with the mean  $T_{\text{eff}}$  without correcting for reddening. While accounting for reddening makes a significant difference, the maximum correction is nevertheless  $\leq 200$  K when relying on the Hakkila et al. (1997) reddening. As expected, the use of the Schlegel et al. (1998) method would raise the de-reddened  $T_{\text{eff}}$  values greatly in some cases as seen from Table 3. As detailed below, those high  $T_{\text{eff}}$  values are in many cases inconsistent with those estimated independently from  $\text{H}\alpha$  line-profile fitting.

The typical observational error in  $(b - y)$  is 0.007 mag, which according to Eq. 2 corresponds to an error in  $T_{\text{eff}}$  of about  $\pm 35$  K, assuming an associated uncertainty in  $[\text{Fe}/\text{H}]$  of  $\pm 0.1$  dex. The observational error in  $(V - K)$  is significantly higher, perhaps as high as  $\pm 0.05$  mag, but due to the high sensitivity to  $T_{\text{eff}}$  for this colour, this corresponds to only  $\pm 45$  K. These errors are consistent with the spread in the difference between the two colour indicators as shown in Fig. 3. The absolute  $T_{\text{eff}}$  values are, however, likely significantly more uncertain than this. Another important uncertainty stems from the adopted reddening, which is hardly better determined than  $\Delta E_{(B-V)} = \pm 0.02$  ( $\Delta E_{(b-y)} = \pm 0.014$ ). This error estimate may even seem optimistic in view of the large error (0.07 mag.) quoted by Hakkila et al. (1997). However, the relatively small

distances to our programme stars as well as the small reddening values from both Hakkila et al. (1997) and Schlegel et al. (1998) support such a low value. This corresponds to an error in  $T_{\text{eff}}$  of about  $\pm 70$  K. Furthermore,  $T_{\text{eff}}$  may be affected by other systematic errors, but a reasonable estimate of the uncertainty in  $T_{\text{eff}}$  is  $\pm 100$  K.

### 3.4. Effective temperature: hydrogen lines

The stellar  $\text{H}\alpha$  656.3 nm line is a potentially good indicator of effective temperatures and has been used extensively in the literature (e.g. Fuhrmann et al. (1993); Barklem et al. (2002) and references therein). The fact that this temperature indicator is not affected by reddening is an advantage over photometry-based methods, especially when accurate reddening estimates are not available. As discussed in detail by Barklem et al. (2002) there are, however, several problems with this methods which must be overcome. An important aspect to be considered in the modelling is the theory used to describe the broadening of the hydrogen lines, both Stark and self-broadening. Additionally, the results are dependent on the employed 1D model atmospheres with the mixing length parameters used for computing the convective energy flux (Fuhrmann et al. 1993). One may worry that the 1D model atmospheres are not sufficiently realistic to describe this aspect. There is also some dependence of  $T_{\text{eff}}$  as derived from H lines on the adopted stellar gravities. A change of 0.3 dex in  $\log g$  can affect the estimates of the effective temperatures by as much as 60 K in the case of the metal-poor subgiants. Finally, the normalisation of the observed spectra is also a potential source of error. However, for our subgiants, the wings of the  $\text{H}\alpha$  line do not extend more than one spectral order so the normalisation of the spectra, though not trivial is much less a critical issue than when dealing with turn-off stars. Furthermore, given the metal-poor nature of our targets, it is straightforward to trace the hydrogen wings between the very few other stellar lines in this wavelength region.

Our spectra are of sufficiently high quality in terms of resolving power and  $S/N$  so that the observational errors in the H line profiles are insignificant compared with the modelling uncertainties (broadening and model atmospheres in particular). We estimate that our relative  $\text{H}\alpha$ -based  $T_{\text{eff}}$  values are accurate to significantly better than 100 K, although the absolute values could be in error by perhaps twice this amount (see discussion in Barklem et al. 2002). As a consequence, the  $\text{H}\alpha$  method mainly serves here as an independent test of the photometric values derived above, which will remain our preferred choice for the abundance analysis.

The observed  $\text{H}\alpha$  lines are displayed in Fig. 4 for five stars together with corresponding synthetic spectra. The theoretical H line profiles shown in the figure have been computed for the mean de-reddened  $T_{\text{eff}}$  based on  $(b - y)$  and  $(V - K)$  as well as for  $T_{\text{eff}} \pm 100$  K. We note that we only attempt to fit the wings of the H line as the core

is affected by departures from LTE (Przybilla & Butler 2004) and by uncertainties in the structure of the upper atmosphere and its velocity fields. Estimates of effective temperatures based on  $H\alpha$  are given in Table 3. They agree with the assumed photometric stellar effective temperatures to within 100 K except for HD 45282 and CD-24° 1782. A lower effective temperature had to be adopted to fit their observed  $H\alpha$  lines, 5050 K and 4900 K versus 5352 K and 5228 K. The computed spectra for those new effective temperature values are shown in Fig. 5.

Estimates of effective temperatures based on  $H\alpha$  lines are in this work on average about 70 K lower than the values based on photometry associated with reddenings from Hakkila et al. (1997) and about 10 K higher than values based on the non-corrected photometry. There is no obvious trend in the differences of  $H\alpha$  temperatures and the photometric ones with the assumed reddening. On the other hand, the values of  $T_{\text{eff}}$  coming from de-reddened photometry using reddenings from Schlegel et al. (1998) are higher by about 150 K than the values determined from  $H\alpha$ . This is another indication that the Schlegel et al. dust maps overestimate the reddenings for our programme stars.

### 3.5. Gravities

The stellar surface gravities were determined from Hipparcos parallaxes as long as the relative error  $\Delta\pi/\pi$  in the parallax satisfied  $\Delta\pi/\pi \leq 0.5$ . This was fulfilled in all cases except for HD 126587 and CD-30° 0298. To convert from parallaxes to surface gravities we relied on the fundamental relation (e.g. Nissen et al. 1997):

$$\log \frac{g}{g_{\odot}} = \log \frac{M}{M_{\odot}} + 4 \log \frac{T_{\text{eff}}}{T_{\text{eff}\odot}} + 0.4V_0 + 0.4BC + 2 \log \pi + 0.12. \quad (4)$$

The stellar mass  $M$  was assumed to be  $0.8 M_{\odot}$  for all stars which, however, is not a critical assumption for this method. The bolometric corrections  $BC$  were taken from Bessell et al. (1998). The estimates of the surface gravities based on Eq. 4 are presented in Table 3. The main source of error for the stellar gravities based on this method is in most cases the adopted parallaxes. We estimate the total uncertainty in surface gravity by adding in quadrature the errors due to the quoted errors in Hipparcos parallaxes (see Table 1), an uncertainty of 100 K in  $T_{\text{eff}}$  and  $0.05 M_{\odot}$  in mass. These  $1\sigma$  errors are also listed in Table 3. We note that the effects of uncertain reddening are small as they affect  $T_{\text{eff}}$  and visual magnitude in opposite directions and therefore mainly cancel each other. The typical uncertainty in  $\log g$  is  $\pm(0.2 - 0.4)$ .

An independent method of deriving surface gravities relies on the use of theoretical evolutionary isochrones for the assumed mass. We have used this method as a test, and it is our main method for the two stars HD 126587 and CD-30° 0298 without reliable Hipparcos parallaxes.

We used the isochrones of Bergbusch & Vandenberg (2001), which are based on the evolutionary tracks of Vandenberg et al. (2000). Interpolation of the isochrones in  $\alpha$ -enhancement and in metallicity was performed, adopting 0.4 and 12 Gy for the  $\alpha$ -enhancement and age, respectively, for all the stars. As corresponding theoretical isochrones are not available for  $[\text{Fe}/\text{H}] \leq -2.31$ , the isochrone calculated for the lowest metallicity was adopted for HD 126587 and CD-30° 0298 which are both quite metal poor, as well as for HD 200654 ( $[\text{Fe}/\text{H}] = -2.75$ ). The rest of our programme stars have metallicities of about  $-2.3$  or higher.

The resulting surface gravities based on isochrone fitting are listed in Table 3. Fig. 6 shows a comparison of the isochrones with the surface gravities estimated from Hipparcos parallaxes. As can be seen, the agreement with the stars for which accurate parallaxes are available are quite good. The mean difference in  $\log g$  amounts to  $0.21 \pm 0.13$ . We have used these differences to correct the isochrone-based values for HD 126587 and CD-30° 0298 to place them on the same scale as the other stars which are based on Hipparcos parallaxes. The mean difference for the six stars with  $[\text{Fe}/\text{H}] \leq -2.2$  is  $\Delta \log g = 0.22 \pm 0.50(\text{s.d.})$ . The final  $\log g$  values for these two stars listed in Table 3 have thus been corrected by 0.22. The error in logarithmic gravity for these stars is estimated to be  $\pm 0.5$ . Fortunately, the method seems to be rather insensitive to metallicity.

### 3.6. Metallicity and microturbulence

The procedure to determine spectroscopic stellar parameters must be iterative. The effective-temperature and surface-gravity estimates depend on the adopted stellar metallicity, which in turn depends on the other two parameters. We used the Strömgren  $m_1$  index to obtain a starting guess for the metallicity of the model atmosphere by which we derived new  $[\text{Fe}/\text{H}]$  values using observed Fe II lines. We have employed the same 13 Fe II lines as in Nissen et al. (2002) with the same adopted line properties. These new  $[\text{Fe}/\text{H}]$  values were subsequently used to derive new  $T_{\text{eff}}$  and  $\log g$  values for the stars. New MARCS model atmospheres were computed with these new parameters from which revised  $[\text{Fe}/\text{H}]$  estimates were calculated. The procedure was repeated until convergence which occurred within a few iterations. The spectroscopic metallicity corresponding to the last iteration was adopted as the final stellar metallicity (Table 4). We note that these values slightly differ from those listed in Table 3, which correspond to the assumed model atmosphere metallicity for the last iteration.

It should be noted that while knowledge about the stellar microturbulence is necessary in this iterative procedure, the exact choice for this parameter is not important for the majority of our stars. Only for the three most metal-rich stars in the sample (HD 274939, HD 218857 and HD 45282) did the derived Fe II-based abundances depend

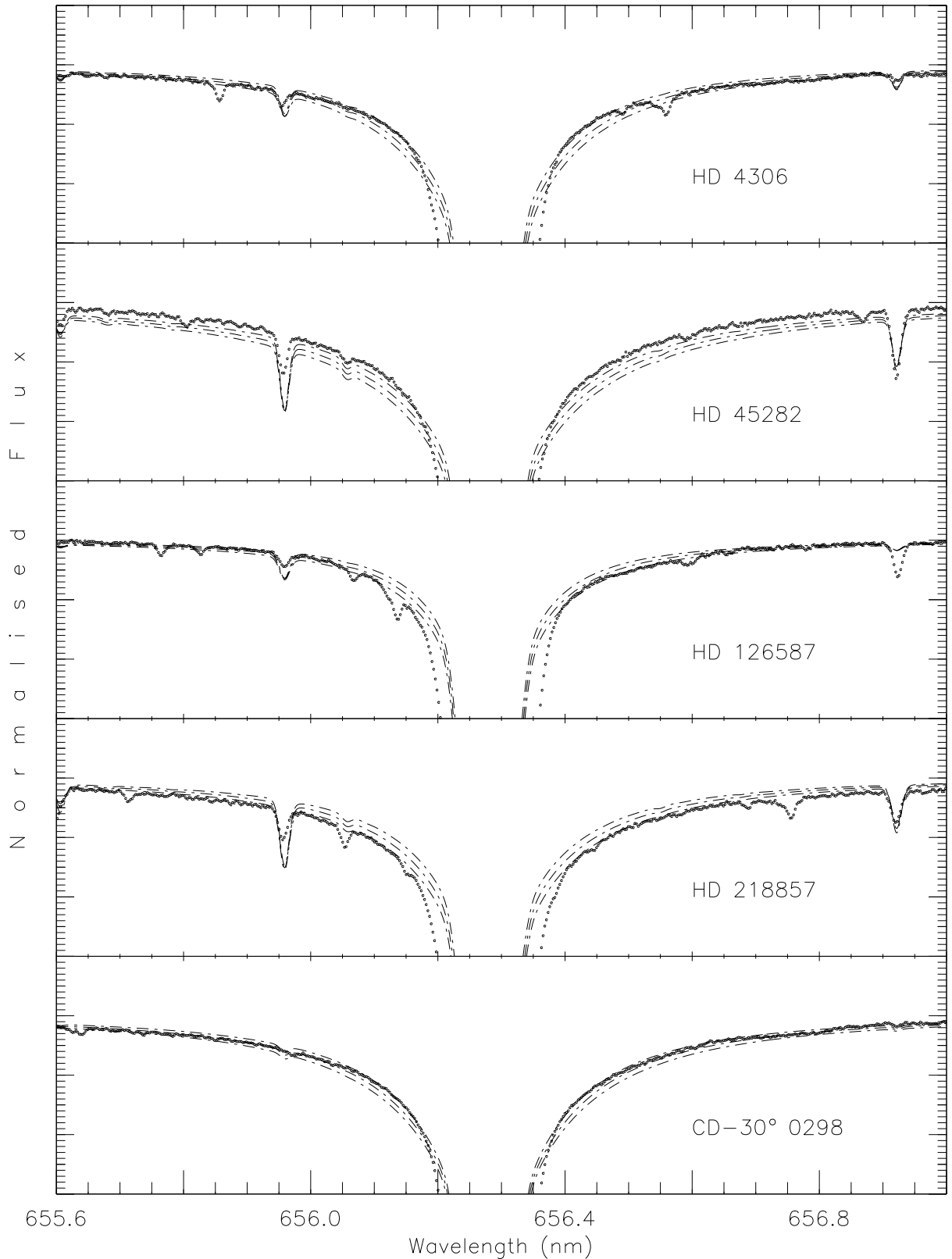


**Fig. 4.** The observed (open circles) H $\alpha$  line spectra are compared for five stars with synthetic spectra (dashed lines). All spectra have been normalised. Three synthetic spectra are plotted for each star, corresponding to three different effective temperatures. The middle line corresponds to the assumed effective temperature based on the de-reddened photometry while the other two correspond to 100 K higher and lower  $T_{\text{eff}}$ , respectively. The scale on the vertical axis goes from 0.7 to 1.1 for each panel. The observed absorption lines in the wings of the H $\alpha$  line which do not have a



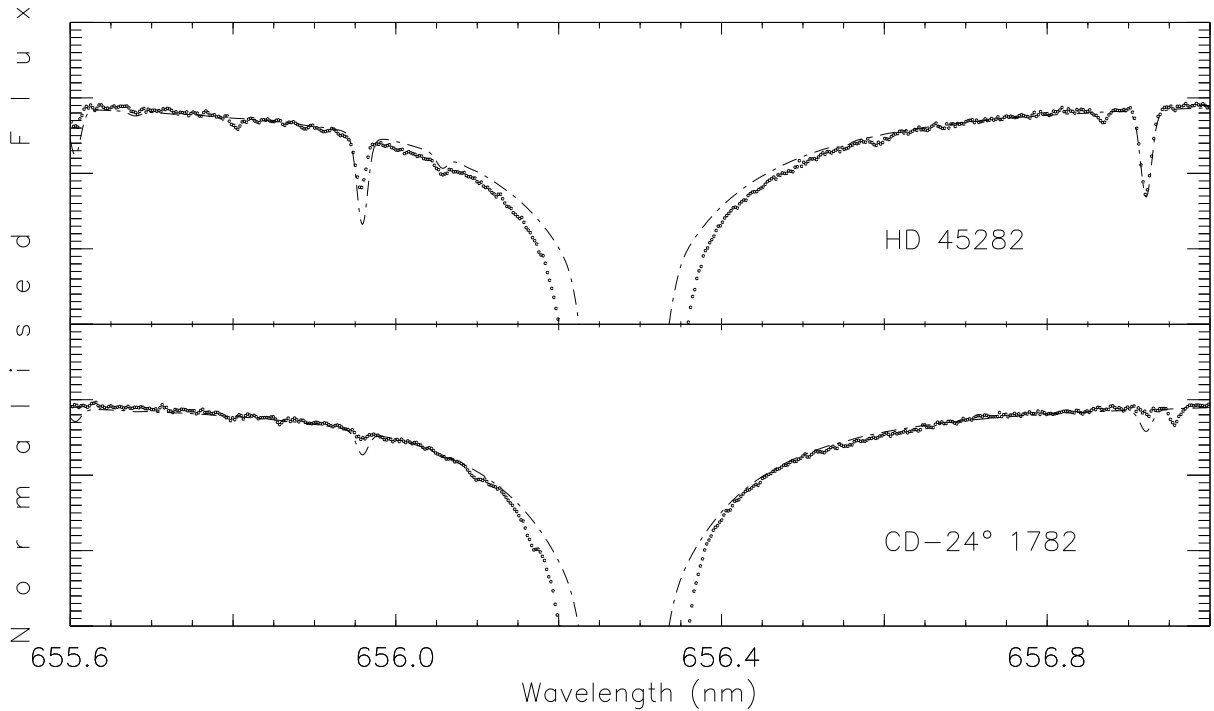


**Fig. 5.** The observed  $H\alpha$  line (circles) and the best-fitting synthetic spectra (dot-dashed lines) for HD 45282 and CD-24° 1782, corresponding to  $T_{\text{eff}} = 5050$  K and 4900 K, respectively.

**Table 4.** The derived  $[\text{Fe}/\text{H}]$  values based on Fe II lines with line-to-line scatter given. Also listed are the associated errors in  $[\text{Fe}/\text{H}]$  due to uncertainties in stellar parameters (100 K for  $T_{\text{eff}}$ , 0.1 dex in  $[\text{Fe}/\text{H}]$  and the errors in  $\log g$  as given in Table 3). Finally, the impact of a measurement error of 0.05 pm for the Fe II equivalent widths on the derived Fe abundances is also illustrated.

| Star        | $[\text{Fe}/\text{H}]$ | $\Delta[\text{Fe}/\text{H}]$ |                 |                              |                      |                       |
|-------------|------------------------|------------------------------|-----------------|------------------------------|----------------------|-----------------------|
|             |                        | $\Delta T_{\text{eff}}$      | $\Delta \log g$ | $\Delta[\text{Fe}/\text{H}]$ | $\Delta W_{\lambda}$ | $-\Delta W_{\lambda}$ |
| HD 4306     | $-2.33 \pm 0.07$       | -0.01                        | 0.10            | 0.01                         | 0.07                 | -0.10                 |
| HD 26169    | $-2.28 \pm 0.04$       | 0.00                         | 0.10            | 0.01                         | 0.06                 | -0.06                 |
| HD 27928    | $-2.14 \pm 0.04$       | -0.01                        | 0.17            | 0.01                         | 0.04                 | -0.06                 |
| HD 45282    | $-1.52 \pm 0.04$       | 0.00                         | 0.05            | 0.02                         | 0.03                 | -0.02                 |
| HD 108317   | $-2.25 \pm 0.04$       | 0.00                         | 0.07            | 0.00                         | 0.05                 | -0.08                 |
| HD 126587   | $-2.87 \pm 0.05$       | 0.00                         | 0.18            | 0.00                         | 0.07                 | -0.10                 |
| HD 128279   | $-2.19 \pm 0.08$       | 0.00                         | 0.07            | 0.00                         | 0.06                 | -0.09                 |
| HD 200654   | $-2.73 \pm 0.08$       | 0.01                         | 0.12            | 0.00                         | 0.08                 | -0.11                 |
| HD 218857   | $-1.79 \pm 0.04$       | -0.02                        | 0.14            | 0.02                         | 0.03                 | -0.03                 |
| HD 274939   | $-1.49 \pm 0.04$       | -0.02                        | 0.13            | 0.02                         | 0.02                 | -0.02                 |
| BD-01° 2582 | $-2.11 \pm 0.07$       | -0.01                        | 0.15            | 0.01                         | 0.05                 | -0.06                 |
| CD-24° 1782 | $-2.25 \pm 0.08$       | -0.01                        | 0.14            | 0.00                         | 0.09                 | -0.10                 |
| CD-30° 0298 | $-3.01 \pm 0.10$       | 0.01                         | 0.19            | 0.00                         | 0.10                 | -0.14                 |

on the microturbulence. The microturbulence parameters for those stars were estimated by requiring that the Fe II lines should not yield any trend in Fe abundance with line strength. The thus estimated microturbulence parameters

were in the range  $1.1 - 1.4 \text{ km s}^{-1}$ . For the other stars, the lines are sufficiently weak to be insensitive to the choice of microturbulence, which were assumed to be  $1.5 \text{ km s}^{-1}$ . The model atmospheres are hardly affected at all by the choice of the parameter.

The equivalent widths of the Fe II lines were measured with the IRAF task *splot*. Due to the weakness of the lines at low metallicity, all 13 Fe II lines were not detected in all stars. In the case of CD-30° 0298 there were only 4 lines detected while at least 11 lines were detected in the spectra of the rest of the stars. The choice of ionized iron lines was natural since these lines are less affected by departures from LTE (such as over-ionization) than neutral iron lines, even if the magnitude of the NLTE effects for Fe I lines is still debated, mainly as a result of the uncertain inelastic H collisions (compare for example the contrasting results of Gratton et al. (1999); Thévenin & Idiart (1999); Korn et al. (2003)). The Fe II lines of our programme stars do not suffer from any apparent blends (Nissen et al. 2002). Iron abundances for each of these lines were derived from the measured equivalent widths adopting the  $gf$ -values of Nissen et al. (2002) which are based on the work by Biemont et al. (1991). The mean abundance was taken as the stellar metallicity. Since we also performed a corresponding solar analysis using the same lines to derive a solar Fe abundance, the effects of any errors in the  $gf$ -values on the stellar iron abundances relative to that of the sun are minimised.

**Table 3.** The derived stellar parameters of our sample. The effective temperatures determined from reddening corrected colour indexes,  $(b - y)_0$  and  $(V - K)_0$ , with reddening values according to column 4 in Table 2. The means of those effective temperatures are presented in the fourth column denoted by  $T_{\text{eff}}$  (adopted). In the fifth column, denoted by  $T_{\text{eff}}$  (no-red), the same type of mean values are reported but with no reddening corrections applied. The mean values for the effective temperatures based on reddenings from Schlegel et al. (1998) are listed in the sixth column. In the seventh column values for effective temperature based on the  $\text{H}\alpha$  line profiles are listed. The remaining columns give values adopted for the model atmospheres for gravities (based on Hipparcos parallaxes and isochrones, respectively), metallicities and microturbulence parameters.

| <i>Star</i> | $T_{\text{eff}}(b - y)$ | $T_{\text{eff}}(V - K)$ | $T_{\text{eff}}$ | $T_{\text{eff}}$ | $T_{\text{eff}}$ | $T_{\text{eff}}(\text{H}\alpha)$ | $\log g$    |            | [Fe/H] | $\xi_{\text{turb}}$    |
|-------------|-------------------------|-------------------------|------------------|------------------|------------------|----------------------------------|-------------|------------|--------|------------------------|
|             | Hakkila et al.          | Hakkila et al.          | adopted          | no-red           | Schlegel et al.  |                                  | Hipparcos   | Isochrones | [dex]  | [ $\text{km s}^{-1}$ ] |
|             | [K]                     | [K]                     | [K]              | [K]              | [K]              | [K]                              | [cgs]       | [cgs]      |        |                        |
| HD 4306     | 5021                    | 4958                    | 4990             | 4890             | 5024             | 4940                             | 3.04±0.26   | 2.14       | -2.35  | 1.5                    |
| HD 26169    | 4962                    | 4982                    | 4972             | 4906             | 5181             | 4972                             | 2.49±0.26   | 2.10       | -2.29  | 1.5                    |
| HD 27928    | 5040                    | 5047                    | 5044             | 4976             | 5078             | 5044                             | 2.67±0.43   | 2.33       | -2.16  | 1.5                    |
| HD 45282    | 5390                    | 5314                    | 5352             | 5208             | 8170             | 5050                             | 3.15±0.13   | 3.44       | -1.53  | 1.1                    |
| HD 108317   | 5301                    | 5300                    | 5300             | 5263             | 5338             | 5300                             | 2.76±0.22   | 3.05       | -2.27  | 1.5                    |
| HD 126587   | 4694                    | 4730                    | 4712             | 4590             | 4907             | 4812                             | (1.66±0.50) | 1.44       | -2.88  | 1.5                    |
| HD 128279   | 5347                    | 5325                    | 5336             | 5151             | 5533             | 5236                             | 2.95±0.21   | 3.16       | -2.21  | 1.5                    |
| HD 200654   | 5306                    | 5278                    | 5292             | 5216             | 5331             | 5192                             | 2.86±0.35   | 3.01       | -2.75  | 1.5                    |
| HD 218857   | 5009                    | 5022                    | 5015             | 4982             | 5117             | 4915                             | 2.78±0.36   | 2.39       | -1.80  | 1.4                    |
| HD 274939   | 5144                    | 5036                    | 5090             | 4991             | 5090             | 5040                             | 2.79±0.33   | 2.73       | -1.51  | 1.3                    |
| BD-01° 2582 | 5032                    | 5112                    | 5072             | 5072             | 5142             | 5022                             | 2.92±0.40   | 2.41       | -2.13  | 1.5                    |
| CD-24° 1782 | 5240                    | 5215                    | 5228             | 5155             | 5228             | 4900                             | 3.46±0.35   | 2.82       | -2.27  | 1.5                    |
| CD-30° 0298 | 5175                    | 5216                    | 5196             | 5158             | 5234             | 5044                             | (2.93±0.50) | 2.71       | -3.04  | 1.5                    |

**Table 5.** List of Fe I lines used for iron abundances calculations, excitational potential and  $\log gf$  values from O’Brian et al. (1991).

| $\lambda$ | $\chi$ | $\log gf$ |
|-----------|--------|-----------|
| [nm]      | [eV]   |           |
| 613.66    | 2.45   | -1.41     |
| 613.77    | 2.59   | -1.35     |
| 619.16    | 2.43   | -1.42     |
| 623.07    | 2.56   | -1.28     |
| 625.26    | 2.40   | -1.77     |
| 639.36    | 2.43   | -1.58     |
| 641.17    | 3.65   | -0.72     |
| 642.14    | 2.28   | -2.01     |
| 643.09    | 2.18   | -1.95     |

We have estimated the sensitivity of the derived metallicities to the adopted stellar parameters by repeating the analysis with perturbed values for  $T_{\text{eff}}$ ,  $\log g$ , [Fe/H] and  $\xi_{\text{turb}}$ . For this exercise we have used our estimated uncertainties in the various parameters: 100 K for  $T_{\text{eff}}$ , 0.1 dex in [Fe/H] and the quoted errors in  $\log g$  (from Hipparcos parallaxes) given in Table 3. The changes in the [Fe/H] values in each of these cases are listed in Table 4. The dependence of temperature on the line and continuum opacity is such that the Fe II-based abundances are essentially immune to errors in  $T_{\text{eff}}$  ( $\Delta \log \epsilon_{\text{Fe}} \leq 0.02$  dex). Similarly, the resulting impact on the model atmosphere structure by slight changes in metallicity is very small for these metal-poor stars and has virtually no effect on the derived Fe

abundances. However, the uncertainties in the stellar gravities lead to significant errors in the calculated iron abundances. In the worst cases this error may be as large as 0.19 dex for the stars with poorly determined parallaxes, although in most cases the uncertainty is about 0.10 dex. The microturbulence influences only the iron abundance slightly even for the most metal-rich stars. Even a drastic change such as going from 1.1  $\text{km s}^{-1}$  to 1.7  $\text{km s}^{-1}$  in the case of HD 45282 makes a difference of a mere 0.04 dex in [Fe/H].

Another source of error for the Fe abundances is the measured equivalent widths, in particular given the weakness of some of the employed lines in the most metal-poor stars. Based on photon statistics and the measured  $S/N$  around the Fe II lines we estimate that the uncertainties in the equivalent widths are at most about 0.05 pm. New Fe abundances with such errors added to the measured line strengths were derived and are also listed in Table 4. Fortunately, in all cases such uncertainties in the measured equivalent widths only correspond to errors in the derived mean Fe II abundances of  $\leq 0.14$  dex even in the unrealistic case when all Fe II lines are affected fully and in the same direction.

In the literature and so often, one can find iron abundances for metal-poor solar type stars derived from neutral iron lines rather than from ionised lines. The neutral lines are easier to detect because they are in general stronger than the ionised lines. However, these lines may suffer from departures from LTE in the line formation (Gratton et al. (1999); Thévenin & Idiart (1999); Asplund (2005); Collet et al. (2005)) so we would expect

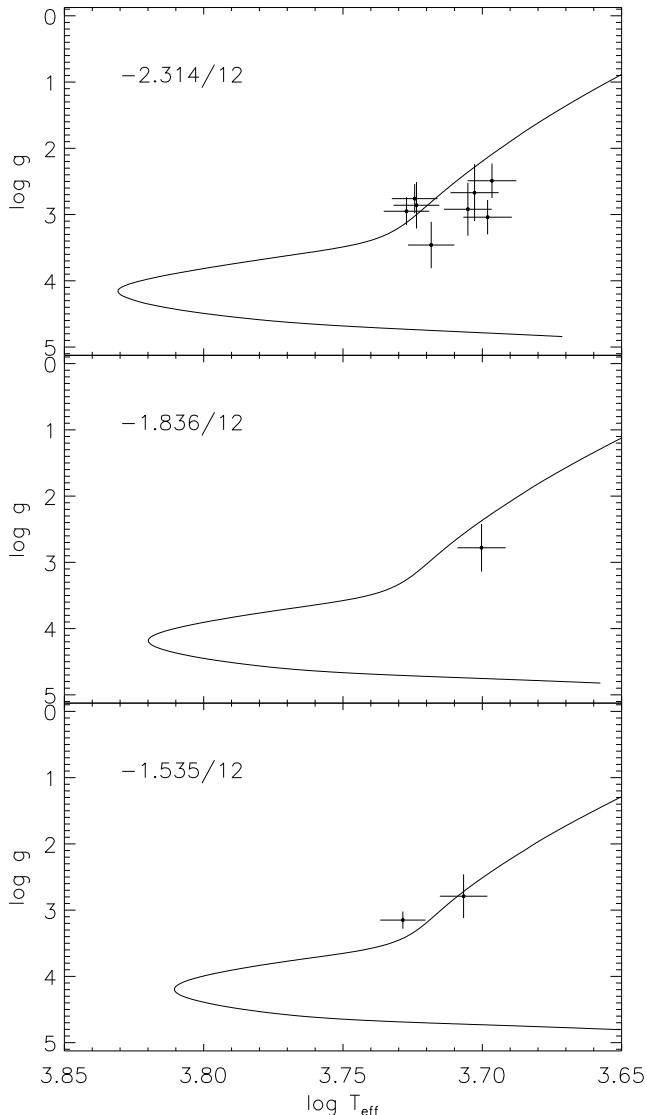


**Fig. 6.** Comparison of the stellar gravities from Hipparcos parallaxes with isochrones from Bergbusch & Vandenberg (2001). The three panels display the results for three difference metallicities:  $[\text{Fe}/\text{H}] = -2.31, -1.84$  and  $-1.54$ . In each case the isochrone at an age of 12 Gyr has been used. The stellar data in the  $[\log g, \log T_{\text{eff}}]$  plane are represented by circles with crosses denoting the estimated errors. The stars are distributed between the panels according to their metallicities.

abundances derived from them to be different from the iron abundances derived from Fe II lines. We investigated this by deriving iron abundances from the measured equivalent widths of a set of Fe I lines (see Table 5). A trend may exist for abundance differences between Fe I and Fe II lines with the assumed metallicity; lower metallicities seem to show larger differences. On average, our assumed metallicity values are 0.2 dex higher than the values derived from the neutral lines (see Table 6), except for two stars (HD 45282 and HD 128279). Furthermore, we note that two of the most metal-poor stars of our sample show the

**Table 6.** Stellar iron abundances determined from the Fe I lines in Table 5. Last column reports Fe I–Fe II iron abundance differences.

| <i>Star</i> | $\log \epsilon_{\text{Fe}}$ | $\Delta \log \epsilon_{\text{Fe}}$<br>(Fe I–Fe II) |
|-------------|-----------------------------|--|
| HD 4306     | 4.65                        | −0.56  |
| HD 26169    | 5.04                        | −0.23  |
| HD 27928    | 5.17                        | −0.24  |
| HD 45282    | 6.30                        | 0.26   |
| HD 108317   | 5.24                        | −0.05  |
| HD 126587   | 4.41                        | −0.26  |
| HD 128279   | 5.39                        | 0.04   |
| HD 200654   | 4.69                        | −0.11  |
| HD 218857   | 5.53                        | −0.23  |
| HD 274939   | 5.99                        | −0.07  |
| BD−01° 2582 | 5.12                        | −0.32  |
| CD−24° 1782 | 4.84                        | −0.46  |
| CD−30° 0298 | 4.22                        | −0.30  |

largest differences (HD 4306 and CD−24° 1782). The fact that Fe II-based metallicities are lower than the ones derived from Fe I lines is not easy to explain in terms of the NLTE effects because Fe I lines should give lower values than Fe II lines.

Let’s now take a closer look at those objects sticking out of the general trend, i.e. the two stars for which the iron abundances derived from Fe II lines are lower than those derived from Fe I lines, and the two metal-poor stars with the largest Fe I–Fe II differences. The first possible source of the observed discrepancy are the stellar parameters, which could have been wrongly determined for these four stars. In the case of HD 45282 and HD 128279, we note they have the highest  $T_{\text{eff}}$  of the entire sample, as well as the largest assumed reddening. This may clearly indicate that our effective temperatures for these two stars have been overestimated. Indeed, a decrease of 100 K in their temperatures (at the border-line of our quoted uncertainty on this stellar parameter) would bring Fe I and Fe II abundances in satisfactory agreement (within 0.1 dex), although with opposite sign. For the latter two stars, HD 4306 and CD−24° 1782, we note that their Hipparcos-based gravities are much higher than the values derived for stars of similar stellar characteristics. Again, this could be a hint that our gravity estimates for these two stars are not the optimal values, which could well explain the very large differences observed between Fe I- and Fe II-based abundances (up to 0.5 dex!). If we were to lower their gravity values to, e.g., 2.5 and 3.0 respectively (from 3.04 and 3.46, but still within a two sigma error), we would then derive a Fe I–Fe II abundance difference of the order of 0.3 dex which is in more accordance with the average value we find (0.2 dex). Note that the isochrones-based gravity values for both stars are even lower than 2.5 and 3.0, which would lead to an even better agreement between Fe I and Fe II.

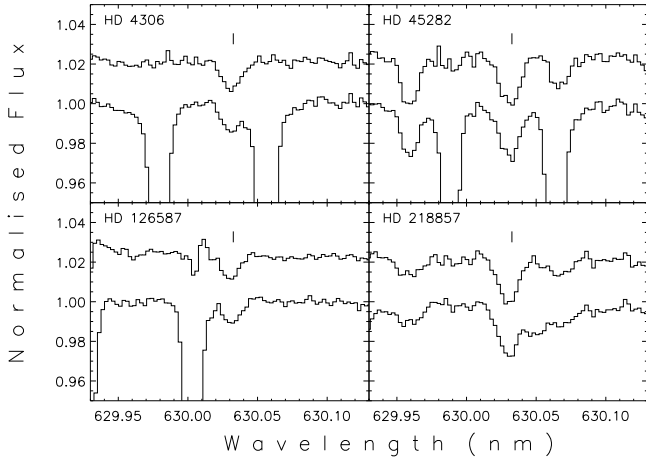


**Fig. 7.** Observed spectra with the forbidden [O I] line at 630.03 nm marked with a vertical bar for four of the programme stars. The appearance of the spectra before and after correction for telluric absorption is shown; the corrected spectra were re-scaled along the vertical scale.

#### 4. Oxygen abundances

In general it is reasonable to assume that the more different types of abundance indicators are being used, the more reliable are the results, provided that the various transitions yield consistent results. There are four different indicators for stellar oxygen abundances, three of which are located in the wavelength range covered by UVES. In essentially all previous work in the extensive literature on oxygen abundances in metal-poor stars, the abundances have been derived from only one or in some cases two of these indicators simultaneously. We have chosen to target subgiants and giants near the base of the red giant branch at exceptionally high  $S/N$  both in the UV and optical regions with the aim to exploit the unique opportunity to derive abundances from three basically different abundance indicators.

In this section we describe how the oxygen abundances have been derived for the different types of lines. In the case of the forbidden [O I] and the O I IR triplet lines we have employed both the techniques of measuring equivalent widths and detailed spectrum synthesis, while only the latter is feasible for the crowded spectrum around the OH UV lines. The equivalent widths have been measured using the IRAF task called *splot*, either by directly integrating the area of the spectral line of interest or by fitting the spectral lines with a Gaussian or another type of function and then integrating that curve. As the  $S/N$  of our spectra is superb, the direct integration method is in general preferred, since a Gaussian can not perfectly describe a stellar spectral line due to the line asymmetries induced by the convective motions in the stellar atmosphere. In a few occasions a Gaussian fit had to be adopted due to presence of telluric lines disturbing the profile of the [O I] line.

#### 4.1. Solar abundances

In order to obtain accurate [O/Fe] values for the stars, we must also derive consistent solar O and Fe abundances. The solar iron abundance was determined from each of the 13 Fe II lines used to derive the stellar Fe abundances with transition probabilities and equivalent widths from Nissen et al. (2002), measured in the solar flux atlas of Kurucz et al. (1984). The solar analysis proceeded completely analogously to the stellar Fe determinations. The thus derived solar Fe abundance is  $\log \epsilon_{\text{Fe}} = 7.56 \pm 0.09$  (standard deviation). The absolute abundance is reasonably close to the quoted meteoritic abundances of 7.50 in Grevesse & Sauval (1998) and 7.45 in Asplund (2005). Indeed, had the oscillator strengths from VALD been adopted for these lines, solar iron abundance would have decreased to 7.44 while the line-to-line dispersion diminished to 0.05 dex. The relatively high scatter among the different lines is similar to that achieved in the 3D analysis of solar Fe II lines by Asplund et al. (2000), and presumably mainly reflects errors in the oscillator strengths. Minor sources of error are inaccurate equivalent widths and departures from LTE in the line formation. Unlike for our metal-poor stars, in the solar case the Fe II lines of interest are sufficiently strong (2.0-9.0 pm with 9 lines  $< 4.5$  pm) that errors in line broadening may also play a role. If the Unsöld enhancement factor for the van der Waal's broadening were changed from 1.5 to 2.0 the solar iron abundance would only change by 0.015 dex. Much more important is the impact of the microturbulence: the metallicity changed by  $-0.16$  dex when the assumed value of microturbulence was altered from 1.15 to 2.00  $\text{km s}^{-1}$ . By computing [Fe/H] values for each individual line for the stars in our sample, we removed much of the uncertainty in the  $gf$ -values and could thus achieve a considerably reduced line-to-line scatter ( $\leq 0.05$  dex for seven of our stars and only in one case as high as 0.10 dex).

A solar O abundance was determined from the [O I] 630.03 nm line using the measured equivalent width of 0.55 pm from Nissen et al. (2002). The 636.38 nm line is more severely blended and was not used. As also the [O I] 630.03 nm line is blended, with a Ni I line (Allende Prieto et al. 2001), we have subtracted its contribution from the feature by adopting a solar Ni abundance of  $\log \epsilon_{\text{Ni}} = 6.25$  (Grevesse & Sauval 1998) and  $\log gf = -2.31$  (Allende Prieto et al. 2001). The remaining equivalent width of 0.41 pm attributable to the [O I] 630.03 nm line implies a solar O abundance of  $\log \epsilon_{\text{O}} = 8.74$ . That value was always taken as the solar O abundance independently of the type of indicator used when deriving [O/Fe] for the programme stars.

#### 4.2. Oxygen abundances from the [O I] 630.03 nm line

Oxygen abundances were derived from the [O I] 630.03 nm line using both measured equivalent widths and by means of spectrum synthesis. The measured equivalent widths are given in Table 7. Depending on the radial velocity of

the star the stellar line can be blended by telluric lines which have to be carefully considered, in particular for these metal-poor stars for which the stellar line is so weak. As mentioned in Sect. 2, precautions were taken to avoid such blends and only in one case, for CD-24° 1782, the [O I] line turned out to be so severely blended that it was useless for abundance determinations.

In six additional cases telluric lines partially blended the oxygen feature. In the spectra of these six stars we used the IRAF task *telluric*. However, since the  $S/N$  values for these B stars were lower than for the programme stars, this method degrades the  $S/N$ , and consequently should be avoided if possible. The procedure worked very well for HD 4306, HD 26169, HD 218857 and HD 45282, but less satisfactorily for HD 126587 and HD 128279. The residuals (i.e. the difference between the observed and the calculated spectra, normalised to the continuum) for these two latter stars were not insignificant, being of the order of 1-2%, so equivalent widths were not measured from them. Instead, a Gaussian profile was fitted to the observed lines to estimate the contribution of the blend to the wings. In the case of HD 126587 and contrary to the case of HD 128279, the large residuals are due to a large difference in airmass between the star and the corresponding calibration star, which makes the telluric correction more uncertain. Another reason was that the observations were taken at different times during the night for the programme star and for its comparison star. It should be noted that in the successful cases, blending by telluric lines is not particularly problematic and a reliable equivalent width measurement could be obtained even without the *telluric* procedure. This can be seen in Fig. 7 where a few spectra before and after applying the task are plotted. In the remaining stars, there was no need to perform any division with a B star spectrum as no telluric lines were disturbing the forbidden oxygen line. For those spectra, the equivalent widths were measured directly, using direct integration of the area of the feature in the observed spectrum. In the case of CD-30° 0298 and HD 200654 no convincing line detection could be made and only an upper limit to the measured equivalent width of 0.04 pm and 0.08 pm could be placed. The last value is based on a tentative measurement of the equivalent width.

As is obvious from Table 7, the measured equivalent widths are very small, in particular at the lowest [Fe/H]. It is therefore paramount to carefully estimate the uncertainties in these values. From the typical  $S/N$  of 500 around the [O I] 630.03 nm line, we expect an observational error of  $\leq 0.03$  pm. This calculated value is based on the assumption of a Poisson distribution for the signal, considering noise only in the line and not in the continuum. Fortunately, for these metal-poor stars the placement of the continuum is straightforward and does not add significantly to the error. This was demonstrated by performing repeated independent measurements of the equivalent widths by different people. In all cases the rms of these measurements were  $\leq 0.02$  pm.

**Table 7.** The measured equivalent widths of the [O I] 630.03 nm line and the resulting 1D LTE oxygen abundances. The third column gives the oxygen abundances from the measured equivalent widths. The remaining columns describe the errors in the derived abundances resulting from uncertainties in  $T_{\text{eff}}$ ,  $\log g$ , [Fe/H] and of a conservative measurement error of 0.05 pm; the stellar parameter changes are the same as in Table 4. No value is given for CD-24° 1782 since the forbidden line is badly blended by a telluric line. Only an upper limit could be obtained for CD-30° 0298 and HD 200654.

| <i>Star</i> | $W_\lambda$<br>[pm] | $\log \epsilon_{\text{O}}$ |                 | $\Delta \log \epsilon_{\text{O}}$ |                    |                     |       |
|-------------|---------------------|----------------------------|-----------------|-----------------------------------|--------------------|---------------------|-------|
|             |                     | $\Delta T_{\text{eff}}$    | $\Delta \log g$ | $\Delta [\text{Fe}/\text{H}]$     | $\Delta W_\lambda$ | $-\Delta W_\lambda$ |       |
| HD 4306     | 0.25                | 7.14                       | 0.05            | 0.10                              | 0.02               | 0.08                | -0.10 |
| HD 26169    | 0.33                | 7.05                       | 0.06            | 0.10                              | 0.02               | 0.07                | -0.07 |
| HD 27928    | 0.25                | 7.06                       | 0.05            | 0.16                              | 0.02               | 0.08                | -0.10 |
| HD 45282    | 0.41                | 7.72                       | 0.04            | 0.05                              | 0.02               | 0.05                | -0.06 |
| HD 108317   | 0.25                | 7.23                       | 0.07            | 0.07                              | 0.01               | 0.08                | -0.10 |
| HD 126587   | 0.20                | 6.32                       | 0.08            | 0.17                              | 0.01               | 0.10                | -0.12 |
| HD 128279   | 0.11                | 6.96                       | 0.07            | 0.07                              | 0.01               | 0.17                | -0.25 |
| HD 200654   | < 0.08              | < 6.75                     | ...             | ...                               | ...                | ...                 | ...   |
| HD 218857   | 0.37                | 7.33                       | 0.04            | 0.15                              | 0.03               | 0.06                | -0.06 |
| HD 274939   | 0.74                | 7.76                       | 0.01            | 0.11                              | 0.01               | 0.03                | -0.03 |
| BD-01° 2582 | 0.25                | 7.17                       | 0.05            | 0.15                              | 0.02               | 0.08                | -0.10 |
| CD-24° 1782 | ...                 | ...                        | ...             | ...                               | ...                | ...                 | ...   |
| CD-30° 0298 | < 0.04              | < 6.38                     | ...             | ...                               | ...                | ...                 | ...   |

The [O I] line is blended with a Ni I line at 630.04 nm (Allende Prieto et al. 2001). The theoretical equivalent widths for this line were computed for the stellar parameters in Table 3, adopting Ni abundances as the solar abundance  $\log \epsilon_{\text{Ni}} = 6.25$  scaled to the stellar metallicity. We have adopted the  $gf$ -value for the Ni I line given by Allende Prieto et al. (2001). For the most metal-rich stars of our sample, the Ni contribution is only 0.01 pm and much smaller for the remaining stars. Consequently, it is safe to assume that the entire measured equivalent width given in Table 7 is due to oxygen.

The measured equivalent widths have been converted to stellar oxygen abundances by using the LTE spectral line formation code EQWIDTH of the Uppsala spectrum synthesis package, and MARCS theoretical 1D-LTE model atmospheres. The  $gf$ -value for the [O I] line was taken as  $\log gf = -9.72$ , which is the same as adopted by Allende Prieto et al. (2001) and Nissen et al. (2002) in their analyses of the line. The line is in all cases sufficiently weak that uncertainties in the van der Waal's pressure broadening, radiative broadening and microturbulence are completely negligible. The resulting oxygen abundances are given in Table 7.

We have investigated the sensitivity of the derived results to the uncertainties in the stellar parameters. Table 7 gives the oxygen abundances when perturbing the stellar parameters by their typical errors ( $\pm 100$  K in  $T_{\text{eff}}$ , the quoted uncertainties in  $\log g$  in Table 3 and  $\pm 0.1$  in

[Fe/H]). The highest sensitivity is for  $\log g$  where the errors are typically 0.10 dex but can be as large as 0.17 dex. The corresponding errors for  $T_{\text{eff}}$  uncertainties are about 0.05 dex while the derived oxygen abundance is insensitive to the employed [Fe/H]. One of the major advantages with using Fe II lines to estimate [Fe/H] is that the sensitivity of the Fe II and [O I] lines to the stellar parameters is very similar. Indeed, the thus derived [O/Fe] values are practically independent of the choice of  $\log g$  ( $\leq 0.01$  dex) and only moderately sensitive to  $T_{\text{eff}}$  ( $\sim 0.05$  dex). It is therefore clear that our final error budget for [O/Fe] as obtained from the [O I] line will be dominated by the measurement error. Since the abundance error will be dependent on  $\Delta W_\lambda/W_\lambda$ , the estimated (conservative) observational error of 0.05 pm will have the largest impact for the most metal-poor stars in our sample.

Spectrum synthesis was also applied with the aim of checking the oxygen abundances determined from the measured equivalent widths. This was done using the spectrum synthesis code BSYN which is also a part of the Uppsala package. The necessary line broadening due to macroturbulence was determined using nearby Fe II lines. The agreement between the equivalent width and spectrum synthesis values is excellent. The equivalent width-based abundances were finally adopted.

Kiselman (1993) has studied the NLTE line formation of the forbidden oxygen line. According to his calculations, the LTE approximation is perfectly justified. In cool stars such as ours, oxygen is mostly in the ground level of the neutral state because of its high ionization energy and the high energies of the excited atomic levels. The forbidden line is a transition between the ground state and the first excited level of O I, which are closely collisionally coupled. Departures from LTE are therefore insignificant for this line.

#### 4.3. Oxygen abundances from the O I 777.1-5 nm lines

The O I triplet at 777.1-5 nm falls near the edges of two adjacent spectral orders in the UVES standard configurations that we had to use due to the service mode nature of our observational programme. Therefore, while the  $S/N$  is excellent at wavelengths near the centre of the orders, the counts decrease rapidly towards the location of the triplet. Typically we measure  $S/N$  of  $\geq 250$  around the lines but there can be substantial variations for a given order of a star even within the 0.5 nm wavelength range of the three triplet lines. An additional complication is residual fringing which could not be removed fully after flat-fielding.

As for the [O I] line, O abundances were estimated from equivalent widths. The oscillator strengths for the transitions were adopted from Wiese et al. (1996):  $\log gf = 0.369, 0.223$  and  $0.002$  for the 777.19 nm, 777.42 nm and 777.54 nm lines, respectively. For completeness we note that we used the Unsöld formula with an enhancement factor of 2.5 for the van der Waal's pressure broadening of

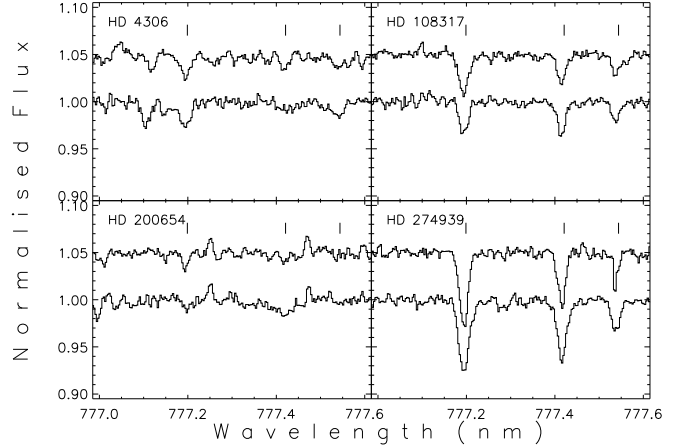


**Fig. 8.** Two adjacent spectral orders containing the O I triplet at 777.1-5 nm, scaled to similar continuum levels. The positions of the triplet lines are indicated by vertical bars.

the lines. This has no impact on the derived abundances given the weakness of the lines. Likewise, even a change in microturbulence by  $1 \text{ km s}^{-1}$  introduces a change in O abundance from the triplet by  $\leq 0.02$  dex.

The equivalent widths of the three triplet lines were measured in both echelle orders for each star. In a few cases, no reliable equivalent width could be measured due to insufficient  $S/N$  or peculiar profiles. The values from the two orders were averaged, weighted with the  $S/N$  of the spectra around the lines. The quality of the spectra in the different spectral orders is illustrated in Fig. 8. Based on the comparison of the two sets of equivalent widths, we estimate that the error in the mean equivalent width is  $\leq 0.1$  pm.

From these equivalent widths, oxygen abundances were derived for each line, which were subsequently averaged to yield the O I triplet-based abundance for the stars. The equivalent widths and the thus derived O abundances are given in Table 8. The three lines normally give consistent abundances with typical line-to-line scatter of 0.08 dex. In one case the largest and smallest values differ by 0.22 dex.

We have investigated the uncertainty in the derived oxygen abundances by varying the stellar parameters and the equivalent widths in the same fashion as for the forbidden oxygen line. The results of this exercise are shown in Table 9. Contrary to the abundances based on the forbidden oxygen line, those based on the triplet lines decrease when the effective temperatures increase due to the high excitation potential of the levels of these lines. The population of the excited levels increases with temperature such that an increase of 100 K in  $T_{\text{eff}}$  results in a decrease of 0.1 dex in abundance. As oxygen is predominantly neutral in the conditions prevailing in the atmospheres of our stars, the O I lines are sensitive to the gravity. Just like for the [O I] line, the abundance sensitivity is about 0.1 dex for the uncertainties of our  $\log g$  estimates. The sensitivity to

**Table 8.** The mean and s.d. of the equivalent widths of the O I 777.1-5 nm triplet lines measured from two different spectral orders and the derived oxygen abundances. The abundances given in columns 5-7 are the equivalent width-based LTE abundances for the three lines with the mean for those and the s.d. listed in column 8. The last column give the abundances corrected for departures from LTE (see text).

| <i>Star</i> | $W_\lambda$      |                  |                  | $\log \epsilon_{\text{O}}$ |             |             |             |      |
|-------------|------------------|------------------|------------------|----------------------------|-------------|-------------|-------------|------|
|             | 777.1 nm<br>[pm] | 777.4 nm<br>[pm] | 777.5 nm<br>[pm] | 777.1 nm                   | 777.4 nm    | 777.5 nm    | NLTE        |      |
| HD 4306     | 0.63 ± 0.16      | 0.24             | 0.39             | 7.46 ± 0.13                | 7.16        | 7.60        | 7.40 ± 0.22 | 7.33 |
| HD 26169    | 0.81 ± 0.08      | 0.53 ± 0.10      | 0.42 ± 0.11      | 7.39 ± 0.05                | 7.32 ± 0.09 | 7.43 ± 0.14 | 7.38 ± 0.05 | 7.31 |
| HD 27928    | 0.67 ± 0.06      | 0.58 ± 0.05      | 0.28 ± 0.08      | 7.28 ± 0.05                | 7.36 ± 0.04 | 7.22 ± 0.13 | 7.29 ± 0.07 | 7.22 |
| HD 45282    | 2.06 ± 0.08      | 1.77 ± 0.23      | 1.17 ± 0.14      | 7.79 ± 0.03                | 7.84 ± 0.09 | 7.81 ± 0.07 | 7.82 ± 0.03 | 7.70 |
| HD 108317   | 0.94 ± 0.13      | 0.69 ± 0.07      | 0.50 ± 0.06      | 7.24 ± 0.07                | 7.23 ± 0.06 | 7.29 ± 0.06 | 7.25 ± 0.03 | 7.17 |
| HD 126587   | 0.46             | 0.35             | 0.15             | 7.09                       | 7.10        | 6.94        | 7.04 ± 0.09 | 6.97 |
| HD 128279   | 1.07 ± 0.33      | 0.62 ± 0.00      | 0.39 ± 0.11      | 7.34 ± 0.17                | 7.21 ± 0.00 | 7.20 ± 0.13 | 7.25 ± 0.08 | 7.17 |
| HD 200654   | 0.31 ± 0.05      | 0.18 ± 0.02      | ...              | 6.74 ± 0.07                | 6.66 ± 0.05 | ...         | 6.70 ± 0.06 | 6.63 |
| HD 218857   | 1.05 ± 0.13      | 1.00 ± 0.12      | 0.57 ± 0.09      | 7.60 ± 0.07                | 7.71 ± 0.07 | 7.63 ± 0.09 | 7.64 ± 0.06 | 7.56 |
| HD 274939   | 2.01 ± 0.35      | 1.39 ± 0.40      | 0.62 ± 0.23      | 7.91 ± 0.13                | 7.81 ± 0.18 | 7.58 ± 0.20 | 7.77 ± 0.17 | 7.67 |
| BD-01° 2582 | 1.03 ± 0.09      | 0.88 ± 0.02      | 0.47 ± 0.04      | 7.57 ± 0.05                | 7.64 ± 0.02 | 7.54 ± 0.03 | 7.58 ± 0.05 | 7.50 |
| CD-24° 1782 | 0.51 ± 0.10      | 0.35 ± 0.06      | ...              | 7.27 ± 0.09                | 7.25 ± 0.07 | ...         | 7.26 ± 0.01 | 7.18 |
| CD-30° 0298 | < 0.2            | ...              | ...              | < 6.68                     | ...         | ...         | < 6.68      | 6.61 |

$\log g$  for the triplet is fortunately largely offset by the similar effect on the Fe II lines when estimating [O/Fe].

The triplet is insensitive to the metallicity of the stellar atmosphere model. Since the triplet is quite weak for the relatively low  $T_{\text{eff}}$  of our stellar sample, in particular for the most metal-poor stars, the derived abundances are sensitive to the errors in the measured equivalent widths. Our errors of about 0.1 pm lead to an abundance error of as much as 0.26 dex for the weakest line in the most metal-poor stars, but more typically 0.05-0.10 dex.

It has since long been established that the O I triplet is affected by departures from LTE in late-type stars (e.g. Kiselman 2001, and references therein). We have estimated the NLTE effects on the derived O abundances by performing specifically tailored statistical-equilibrium calculations for our stars, in an identical fashion to those by Nissen et al. (2002). We have used a 23 level model atom with 43 bound-bound transition and with all 22 O I levels connected to O II by photo-ionization transitions. This is sufficiently extensive to yield reliable results since the line formation of the triplet is anyway largely an equivalent two-level problem. The radiative data comes mainly from the Opacity Project (Cunto et al. 1993). Collisional excitation and ionization with electrons and charge transfer reactions are accounted for but inelastic collisions with H have been neglected (see discussion in Kiselman (2001)). The NLTE calculations have been performed using MULTI version 2.2 (Carlsson 1986) for three different abundances surrounding the LTE based abundances derived from the triplet lines for the stars. From these calculations, NLTE abundance corrections were interpolated and added to the LTE results in Table 8. For our stars, the NLTE abundance corrections typically amount to about  $-0.08$  dex.

**Table 9.** The sensitivity of the oxygen abundances from the O I triplet lines to uncertainties in the stellar parameters and equivalent widths. The stellar parameter changes are the same as in Table 4.

| <i>Star</i> | $\Delta \log \epsilon_{\text{O}}$ |                 |                               |                     |                     |
|-------------|-----------------------------------|-----------------|-------------------------------|---------------------|---------------------|
|             | $\Delta T_{\text{eff}}$           | $\Delta \log g$ | $\Delta [\text{Fe}/\text{H}]$ | $+\Delta W_\lambda$ | $-\Delta W_\lambda$ |
|             | LTE                               |                 |                               |                     |                     |
| HD 4306     | -0.11                             | 0.11            | -0.01                         | 0.09                | -0.13               |
| HD 26169    | -0.10                             | 0.10            | 0.00                          | 0.08                | -0.09               |
| HD 27928    | -0.10                             | 0.17            | -0.01                         | 0.09                | -0.12               |
| HD 45282    | -0.10                             | 0.04            | -0.01                         | 0.02                | -0.03               |
| HD 108317   | -0.09                             | 0.08            | 0.00                          | 0.06                | -0.07               |
| HD 126587   | -0.11                             | 0.22            | 0.00                          | 0.14                | -0.24               |
| HD 128279   | -0.09                             | 0.08            | 0.00                          | 0.07                | -0.09               |
| HD 200654   | -0.09                             | 0.14            | 0.00                          | 0.16                | -0.26               |
| HD 218857   | -0.10                             | 0.13            | 0.00                          | 0.05                | -0.06               |
| HD 274939   | -0.11                             | 0.12            | 0.00                          | 0.04                | -0.05               |
| BD-01° 2582 | -0.10                             | 0.16            | 0.00                          | 0.06                | -0.06               |
| CD-24° 1782 | -0.10                             | 0.14            | -0.01                         | 0.10                | -0.12               |
| CD-30° 0298 | ...                               | ...             | ...                           | ...                 | ...                 |

#### 4.4. Oxygen abundances from the OH UV lines

The high quality of our observed spectra in the UV-blue wavelength region has also enabled the use of the OH (A-X) electronic lines around 310 nm for abundance determination. One of the main problems with these diagnostics is the crowded spectral region they are located in. This necessitates the use of spectral synthesis rather than equivalent widths for deriving oxygen abundances. The high  $S/N$  and resolving power of the blue spectra also allow an accurate placing of the continuum which is a non-trivial task for this region. Furthermore, it makes it easier to dis-

tinguish possible blends. That problem is the least for the most metal-poor stars in our sample where the continuum is relatively easy to locate and blends less disturbing, while the most metal-rich stars are likely to have larger abundance uncertainties due to this. An initial normalisation of the UVES pipeline reduced spectra was done by fitting the upper envelope of the spectra to a cubic spline function in IRAF. A minor re-normalisation around the OH lines was subsequently performed in some cases when the comparisons between the normalised observed and synthetic spectra clearly required it.

The selection of the OH lines to use was based on spectral synthesis for two stars bracketing the metallicity range of our sample, HD 4306 ( $[\text{Fe}/\text{H}] = -2.33$ ) and HD 274939 ( $[\text{Fe}/\text{H}] = -1.49$ ). Only lines which were essentially free of blends and sufficiently strong also in our most metal-poor stars were considered. The theoretical OH wavelengths, excitation potentials and transition probabilities were adopted from the line list of Gillis et al. (2001). Many very weak lines which have no impact on the theoretical spectrum were culled from the original line list to save time in the synthesis, which was carried out with the BSYN code of the Uppsala synthesis package. The data for the atomic lines present in this region were taken from VALD (Piskunov et al. 1995) while the necessary data for the few significant CH lines were taken from the database of Kurucz (1993). The first guess for the element abundances used for the synthesis were the same as in the employed model atmosphere, i.e. solar abundances scaled to the adopted metallicity with an  $\alpha$ -enhancement of 0.4 dex. Individual abundances were adjusted as necessary to obtain the correct strengths of lines. The theoretical spectra were first convolved with a Gaussian appropriate to the instrumental resolving power after which an additional broadening profile, taking care of macroturbulence, rotation etc. was applied. The width of the latter was determined individually for each star by optimising the overall fit between the synthetic and observed spectra both for atomic and molecular lines. In the end we identified seven spectral features between 310 and 330 nm which were suitable for O abundance determinations in metal-poor subgiants and giants near the base of the red giant branch. These are listed in Table 10 together with data for the lines. Two of the features are in fact composed of two OH lines so data for nine lines are given. The OH 316.717 line is partly blended with a CH line, which, however, does not cause any significant problems. The O abundance determined from this line is consistent with the values coming from the other OH lines.

The derived oxygen abundances from each feature are listed in Table 11, together with the mean abundance and standard deviation for each star. Spectral synthesis for all the seven lines together with the observations are displayed in Fig. 9 for four stars. All lines give consistent results, which suggests that unidentified blends are not a significant problem. The typical line-to-line scatter is only about 0.1 dex, and 0.12 dex in the worst case. The observed OH lines of interest fall in general between the

lower and upper solid lines in the figure which are the theoretical predictions corresponding to abundance variation of  $\pm 0.2$  dex.

The scatter can likely be explained by the finite  $S/N$ , possible blends and slightly erroneous  $gf$ -values. Departures from LTE could perhaps also contribute (Hinkle & Lambert 1975) although very little work has been done on NLTE effects for molecular lines of electronic band systems. One would expect, however, that the differential NLTE effects for different OH lines of similar excitation potential and line strength in the case of our lines should be marginal, even in the presence of significant overall departures from LTE in the molecular number densities or line-source functions. We note that there is no clear tendency in LTE abundance differences between results from OH lines with different excitation energies or lines from different vibrational bands.

We have investigated the sensitivity of the derived oxygen abundances to the adopted stellar parameters and different continuum location in the observed spectra within reasonable limits. For the purpose, theoretical curve-of-growths were computed for the stellar parameters of our programme stars. The resulting behaviour is complex as the sensitivity depends both on the stellar parameters and the oxygen abundances. These values were perturbed with  $\Delta T_{\text{eff}} = 100$ ,  $\Delta \log g$  according to the errors quoted in Table 3, and  $\Delta [\text{Fe}/\text{H}] = 0.1$ . The estimated abundance errors are given in Table 12. The derived O abundance is quite sensitive to the adopted  $T_{\text{eff}}$  and  $\log g$ . An increase in  $T_{\text{eff}}$  by 100 K would lead to about 0.2 dex higher O abundances while a 0.2 dex increase in  $\log g$  roughly translates to an decrease in abundance by 0.07 dex. The sensitivity to the metallicity of the model atmosphere is minor. It should be noted that the errors due to  $T_{\text{eff}}$  and  $\log g$  goes in the opposite direction to those of Fe II, which unfortunately makes the derived  $[\text{O}/\text{Fe}]$  even more uncertain. We have studied the sensitivity of the adopted spectrum normalisation in HD 45282, which has one of the highest  $[\text{Fe}/\text{H}]$  in our sample and thus should be the most sensitive to the normalisation. An alternative normalisation by 8%, which is on the order of what is still acceptable, leads to a 0.1 dex difference in the derived O abundance for this star. Clearly, this error is small compared with those associated with the stellar parameters.

The final total errors in the OH-based  $[\text{O}/\text{Fe}]$  abundances were estimated for each star individually by adding in quadrature those from the stellar parameter uncertainties and the error in the mean value of the results of the OH feature fits. Typical resulting values are  $\pm 0.3$  dex.

## 5. Discussion

### 5.1. Comparison between the three different indicators

Our comparison between the results from the three oxygen abundance indicators is made primarily in terms of  $[\text{O}/\text{Fe}]$  which is a key parameter in studies of the chemical



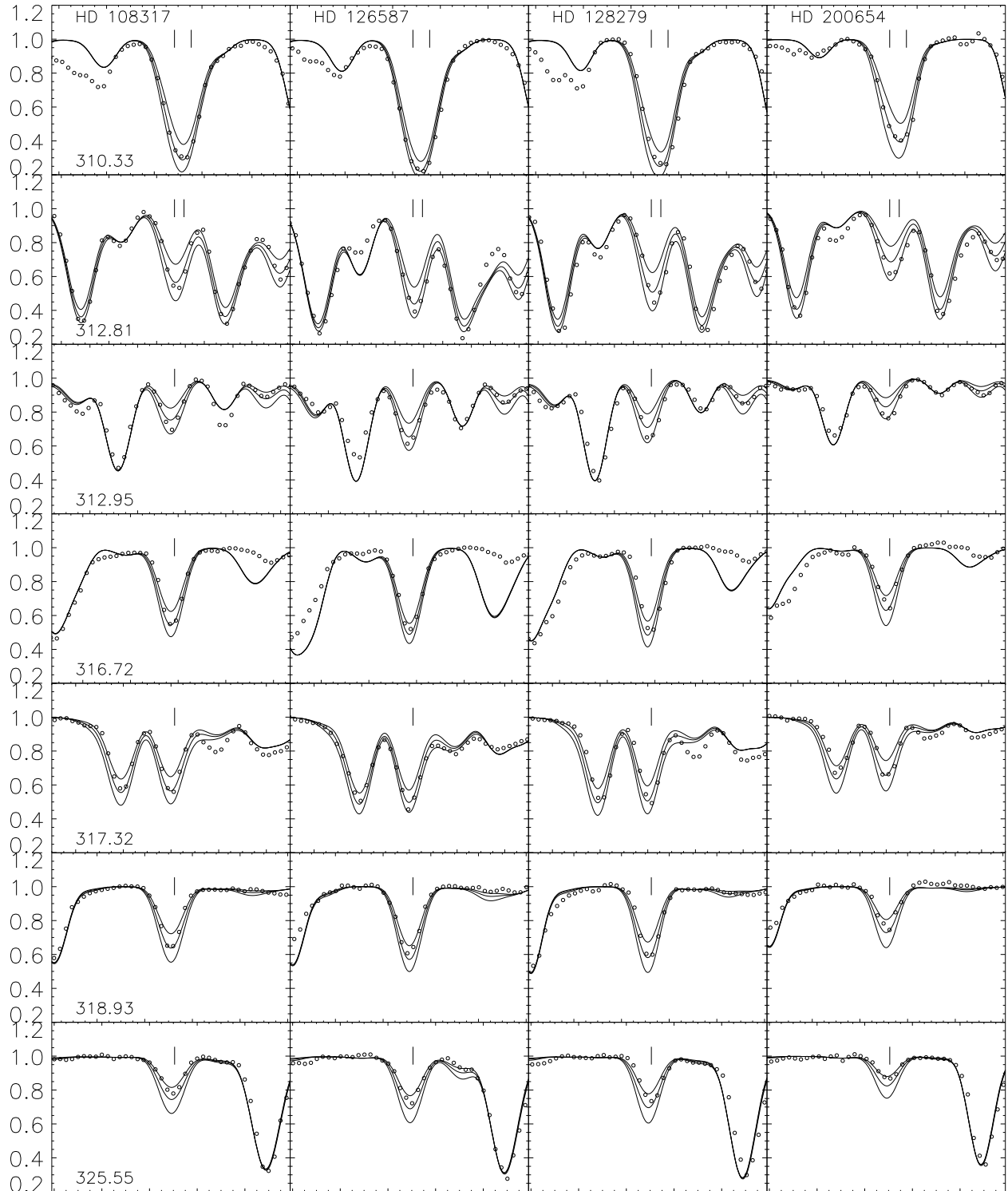


**Fig. 9.** Comparison between observed and synthetic spectra around the lines in Table 10 for HD 108317, HD 126587, HD 128279 and HD 200654, with the synthetic spectra computed for three different abundances: the mean value for each star as listed in Table 11 and these values  $\pm 0.2$  dex. The position of the OH lines used are marked with vertical bars and their wavelengths are given in the respective panel.

**Table 11.** The derived 1D LTE oxygen abundances from the OH lines listed in Table 10. The last column lists the derived mean abundance and its standard deviation (s.d.).

| Star        | $\log \epsilon_{\text{O}}$ |                     |         |         |         |         |         | $\log \epsilon_{\text{O}} \pm s.d.$ |
|-------------|----------------------------|---------------------|---------|---------|---------|---------|---------|-------------------------------------|
|             | 310.327+<br>310.334        | 312.806+<br>312.810 | 312.954 | 316.717 | 317.320 | 318.931 | 325.549 |                                     |
| HD 4306     | 6.65                       | 6.73                | 6.80    | 6.63    | 6.68    | 6.68    | 6.58    | $6.68 \pm 0.07$                     |
| HD 26169    | 6.90                       | 7.00                | 7.00    | 6.90    | 6.97    | 6.89    | 6.82    | $6.93 \pm 0.07$                     |
| HD 27928    | 6.96                       | 7.06                | 7.08    | 6.90    | 6.95    | 6.90    | 6.86    | $6.96 \pm 0.08$                     |
| HD 45282    | 7.85                       | 7.90                | 7.98    | 7.90    | 8.00    | 7.90    | 7.77    | $7.90 \pm 0.08$                     |
| HD 108317   | 7.20                       | 7.30                | 7.33    | 7.25    | 7.25    | 7.22    | 7.15    | $7.24 \pm 0.06$                     |
| HD 126587   | 6.30                       | 6.38                | 6.40    | 6.25    | 6.40    | 6.20    | 6.22    | $6.31 \pm 0.09$                     |
| HD 128279   | 7.30                       | 7.40                | 7.45    | 7.25    | 7.35    | 7.25    | 7.21    | $7.32 \pm 0.09$                     |
| HD 200654   | 6.82                       | 6.97                | 7.02    | 6.82    | 6.82    | 6.82    | 6.70    | $6.85 \pm 0.11$                     |
| HD 218857   | 7.07                       | 7.12                | 7.22    | 7.07    | 7.12    | 7.12    | 7.05    | $7.11 \pm 0.06$                     |
| HD 274939   | 7.51                       | 7.65                | 7.70    | 7.55    | 7.65    | 7.60    | 7.56    | $7.60 \pm 0.07$                     |
| BD-01° 2582 | 6.67                       | 6.82                | 6.85    | 6.78    | 6.75    | 6.75    | 6.75    | $6.77 \pm 0.06$                     |
| CD-24° 1782 | 6.75                       | 6.95                | 6.95    | 6.73    | 6.78    | 6.73    | 6.72    | $6.80 \pm 0.10$                     |
| CD-30° 0298 | 6.33                       | 6.41                | 6.33    | 6.20    | 6.27    | 6.16    | 6.05    | $6.25 \pm 0.12$                     |

**Table 10.** Wavelengths of the selected OH lines from the (A-X) electronic system for oxygen abundance determination, together with their corresponding vibrational numbers, excitation potential and  $\log gf$  value.

| $\lambda$<br>[nm] | $\nu'-\nu''$ | $\chi$<br>[eV] | $\log gf$ |
|-------------------|--------------|----------------|-----------|
| 310.327           | 0 0          | 0.053          | -2.799    |
| 310.334           | 0 0          | 0.053          | -2.355    |
| 312.806           | 1 1          | 0.541          | -2.581    |
| 312.810           | 0 0          | 0.210          | -2.969    |
| 312.954           | 1 1          | 0.516          | -2.679    |
| 316.717           | 0 0          | 1.109          | -1.544    |
| 317.320           | 1 1          | 0.842          | -1.888    |
| 318.931           | 1 1          | 1.032          | -1.843    |
| 325.549           | 0 0          | 1.300          | -1.811    |

**Table 12.** Errors in abundances due to uncertainties in effective temperature of 100 K,  $\Delta T_{\text{eff}}$ , in  $\log g$  as given in Table 3,  $\Delta \log g$ , and in metallicity of 0.1 dex,  $\Delta[\text{Fe}/\text{H}]$ .

| Star        | $\Delta \log \epsilon_{\text{O}}$ |                 |                              |
|-------------|-----------------------------------|-----------------|------------------------------|
|             | $\Delta T_{\text{eff}}$           | $\Delta \log g$ | $\Delta[\text{Fe}/\text{H}]$ |
| HD 4306     | 0.19                              | -0.06           | 0.04                         |
| HD 26169    | 0.21                              | -0.07           | 0.03                         |
| HD 27928    | 0.20                              | -0.12           | 0.03                         |
| HD 45282    | 0.17                              | -0.03           | 0.05                         |
| HD 108317   | 0.22                              | -0.07           | 0.02                         |
| HD 126587   | 0.25                              | -0.19           | 0.02                         |
| HD 128279   | 0.20                              | -0.07           | 0.02                         |
| HD 200654   | 0.17                              | -0.12           | 0.01                         |
| HD 218857   | 0.17                              | -0.07           | 0.06                         |
| HD 274939   | 0.15                              | -0.06           | 0.06                         |
| BD-01° 2582 | 0.20                              | -0.09           | 0.04                         |
| CD-24° 1782 | 0.19                              | -0.09           | 0.04                         |
| CD-30° 0298 | 0.23                              | -0.16           | 0.01                         |

evolution of oxygen in the Galaxy. In this way, effects of errors in the stellar parameters are reduced in cases when derived oxygen and iron abundances respond in similar ways to changes in the parameters, i.e. for the [O I] and O I.

Values of [O/Fe] and their uncertainties are summarised in Table 13. In Fig. 10 and for each indicator separately, these values are shown as a function of metallicity. The values derived from OH (bottom panel) are by far the most uncertain with typical error bars in [O/Fe] of the order of 0.30 dex. About two times smaller than this are [Fe/H] and [O/Fe] error bars associated to the forbidden and permitted O I lines. The effective temperature plays a major role in the determination of accurate [O/Fe] values independently of the indicator used. Gravity only plays a significant role when oxygen abundances are derived from the OH UV lines. Measurement errors in equivalent widths also contribute to the [O/Fe] total error.

For many decades, the accuracy of 1D-LTE [O/Fe] values based on [O I] has been limited by the quality of the observed stellar spectra. With the era of new astronomical instruments, this quality has improved very considerably such that measurements based on the weak forbidden line, when not too weak, now probably give the most reliable estimates of [O/Fe] in metal-poor stars. Here, these estimates are taken as reference for the comparison between the indicators.

According to Table 13, [O/Fe] values based on O I permitted lines (including NLTE corrections) are on average  $0.19 \pm 0.07$  dex higher than the reference values, while values based on OH UV lines are  $0.09 \pm 0.08$  dex lower. The magnitudes of the [O/Fe] uncertainties for the individual stars are of the same order or even higher than these values, except the uncertainties of the [O I]-based [O/Fe]. Notice that in the total error in [O/Fe], uncertainties associated with the analysis of the Fe II lines should be included. These uncertainties, however, affect estimates

**Table 13.** [O/Fe] values and their uncertainties as determined from Fe II lines and the three oxygen indicators: [O I], O I IR and OH UV lines. The values derived from O I IR lines are based on NLTE calculations.

| Star        | [O/Fe] |                         |                 |                              |                      | [O/Fe] |                         |                 |                              |                      | [O/Fe] |                         |                 |                              |
|-------------|--------|-------------------------|-----------------|------------------------------|----------------------|--------|-------------------------|-----------------|------------------------------|----------------------|--------|-------------------------|-----------------|------------------------------|
|             | [O I]  | $\Delta T_{\text{eff}}$ | $\Delta \log g$ | $\Delta[\text{Fe}/\text{H}]$ | $\Delta W_{\lambda}$ | O I    | $\Delta T_{\text{eff}}$ | $\Delta \log g$ | $\Delta[\text{Fe}/\text{H}]$ | $\Delta W_{\lambda}$ | OH     | $\Delta T_{\text{eff}}$ | $\Delta \log g$ | $\Delta[\text{Fe}/\text{H}]$ |
| HD 4306     | 0.73   | 0.06                    | 0.00            | 0.01                         | 0.09                 | 0.95   | -0.10                   | 0.01            | -0.01                        | 0.10                 | 0.27   | 0.21                    | -0.16           | 0.03                         |
| HD 26169    | 0.59   | 0.06                    | 0.00            | 0.01                         | 0.07                 | 0.85   | -0.10                   | -0.00           | -0.01                        | 0.09                 | 0.47   | 0.21                    | -0.17           | 0.02                         |
| HD 27928    | 0.46   | 0.06                    | -0.01           | 0.01                         | 0.09                 | 0.62   | -0.09                   | 0.00            | -0.01                        | 0.11                 | 0.36   | 0.21                    | -0.29           | 0.02                         |
| HD 45282    | 0.50   | 0.04                    | 0.00            | 0.00                         | 0.06                 | 0.48   | -0.10                   | -0.01           | -0.03                        | 0.03                 | 0.68   | 0.17                    | -0.08           | 0.03                         |
| HD 108317   | 0.74   | 0.07                    | 0.00            | 0.01                         | 0.09                 | 0.68   | -0.09                   | 0.01            | -0.01                        | 0.07                 | 0.75   | 0.21                    | -0.14           | 0.02                         |
| HD 126587   | 0.45   | 0.08                    | -0.01           | 0.01                         | 0.11                 | 1.10   | -0.11                   | 0.04            | 0.00                         | 0.20                 | 0.44   | 0.26                    | -0.37           | 0.02                         |
| HD 128279   | 0.41   | 0.07                    | 0.00            | 0.01                         | 0.22                 | 0.62   | -0.09                   | 0.01            | -0.00                        | 0.08                 | 0.77   | 0.21                    | -0.13           | 0.02                         |
| HD 200654   | < 0.74 | ....                    | ....            | ....                         | ....                 | 0.62   | -0.10                   | 0.02            | -0.01                        | 0.22                 | 0.84   | 0.21                    | -0.24           | 0.01                         |
| HD 218857   | 0.38   | 0.06                    | 0.01            | 0.01                         | 0.06                 | 0.61   | -0.09                   | -0.01           | -0.02                        | 0.06                 | 0.16   | 0.19                    | -0.21           | 0.04                         |
| HD 274939   | 0.51   | 0.03                    | -0.02           | -0.01                        | 0.03                 | 0.42   | -0.09                   | -0.01           | -0.02                        | 0.05                 | 0.35   | 0.17                    | -0.20           | 0.04                         |
| BD-01° 2582 | 0.54   | 0.06                    | 0.00            | 0.01                         | 0.09                 | 0.87   | -0.09                   | 0.01            | -0.01                        | 0.06                 | 0.13   | 0.20                    | -0.24           | 0.03                         |
| CD-24° 1782 | ....   | ....                    | ....            | ....                         | ....                 | 0.69   | -0.09                   | 0.01            | -0.01                        | 0.11                 | 0.30   | 0.20                    | -0.23           | 0.04                         |
| CD-30° 0298 | < 0.65 | ....                    | ....            | ....                         | ....                 | < 0.88 | ....                    | ....            | ....                         | ....                 | 0.52   | 0.22                    | -0.34           | 0.01                         |

based on the different criteria identically, and thus do not have any impact on the differences. Typical [O/Fe] error bars are of the order of 0.12, 0.15 and 0.3 dex for the estimates based on [O I], O I and OH UV lines, respectively.

If our  $T_{\text{eff}}$ -scale turns out to be too cool, then both [O I] and O I-based estimates are expected to need modification. An increase of the temperatures by 100 K will bring the two different estimates together because the two indicators respond in opposite directions to these changes, with shifts in [O/Fe] of 0.06 dex and -0.1 dex, respectively. Another way of explaining the differences would be to advocate systematic errors in the equivalent widths. E.g., if we assume that the forbidden and the permitted lines are too strong and too weak, respectively, by their typical equivalent-width uncertainties as estimated above, the [O I]-based [O/Fe] values should be adjusted upwards and the O I-based [O/Fe] values decreased by about the same amount,  $\sim 0.1$  dex, and thus reach agreement. A too cool  $T_{\text{eff}}$ -scale can also lead to underestimated [O/Fe] values when based on abundance determinations from OH but by different amounts than for [O I]. Estimates based on the molecular lines increase faster with effective temperature than estimates based on the forbidden line (0.20 versus 0.06 dex) and hence the two estimates get closer to each other with a hotter temperature scale. The mean difference in [O/Fe] between values based on [O I] and OH, respectively, is lower than the [O/Fe] uncertainties of about 0.20 dex due to gravity errors in the analysis of OH lines.

Unfortunately, the standard deviations in the differences are quite significant in comparison with the mean differences themselves. There are a few stars for which the differences are much higher than the mean value. Fig. 11 even demonstrates possible relations between the differences and the effective temperature; higher effective temperature may suggest a lower difference between abundance ratios from the triplet lines and the forbidden line, respectively. The trend for the abundance difference from

the OH lines and the forbidden line is inverted with respect to this; only the coolest star, HD 126587, seems to break such a trend since it shows a good agreement between the two indicators. Unfortunately, this is not the case for the triplet lines in the spectrum of the same star; this giant has the highest discrepancy (0.65 dex) between abundances from those and from the forbidden line. HD 126587 has also high observational errors in O I-based [O/H], 0.24 dex; these uncertainties together with uncertainties in effective temperature are, however, not high enough to account for the observed differences between results from the two different criteria. The observed equivalent widths of the O I IR triplet lines of this star are so low that ripples or fringing in the observed spectra might have disturbed the measurements, see Fig. 12. In the literature we can find other cases with high discrepancies between the two indicators. E.g., according to Barbuy et al. (2003), the [O/Fe] estimates for the metal-poor giant HD 122563 differ by 0.5 dex.

Differences between the OH-based estimates as compared with those of the forbidden line are compatible with uncertainties in the corresponding [O/Fe] estimates if they are smaller than about 0.3 dex. Typically, an increase in effective temperature by 100 K will increase the estimates by 0.14 dex and reduce the differences relative to the estimates from the forbidden line, as will a decrease in gravity by an amount consistent with the expected errors in this quantity which will increase the estimate by about 0.2 dex. Also, a decrease of the equivalent width of the forbidden line by its maximum error, 0.05 pm, would bring down the [O/Fe] estimates from that line by  $\sim 0.1$  dex. As a result of all this, the differences between the different [O/Fe] estimates of about 0.3 dex would be reduced to zero. There are three data points, representing HD 4306, HD 128279 and BD-01°2582 in the bottom panel in Fig. 11, which depart more than one would expect from the errors in parameters and observations. The differences plotted are

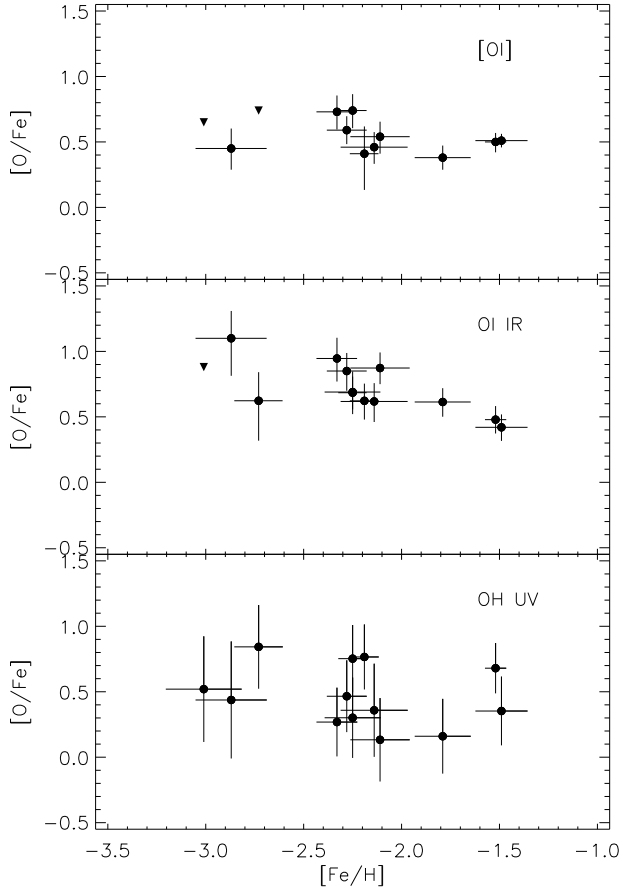


**Fig. 10.**  $[O/Fe]$  estimates as a function of metallicity. Estimates based on different indicators are shown separately:  $[O\text{I}]$  630.03 nm (top panel),  $O\text{I}$  777.1-5 nm (middle panel) and  $OH$  UV 310.0 nm (bottom panel).

negative for two of them while the third one has positive differences (HD 128279).

We remind the reader that our comparison between  $Fe\text{I}$ - and  $Fe\text{II}$ -based iron abundances for HD128279 may suggest that our derived effective temperature has been overestimated (cf Sect. 3.6). If this were the case, then the  $[O/Fe]$  differences plotted in Fig. 11 as well as the scatter in the  $[O/Fe]$ -vs- $[Fe/H]$  trend would be notably reduced (a decrease of 100 K in  $T_{\text{eff}}$  would lower the  $OH$ - and  $[O\text{I}]$ -based  $[O/Fe]$  values by 0.17 dex and 0.04 dex respectively). The case of HD 4306 could be very similar, in the sense that for this star the Hipparcos-based gravity may be too large (see Sect. 3.6). With the newly suggested value of  $\log g = 2.5$ , the  $OH$ -based  $[O/Fe]$  ratios would significantly increase (from 0.27 to 0.6), strongly reducing the abundance difference between the two oxygen indicators.

BD-01° 2582 is claimed to be a CH binary star (Carney et al. 2003) which may explain its departure. If its carbon abundance is very high then most of its oxygen may be in the form of CO and little in the form of OH in its outer atmospheric layers; thus a higher oxygen

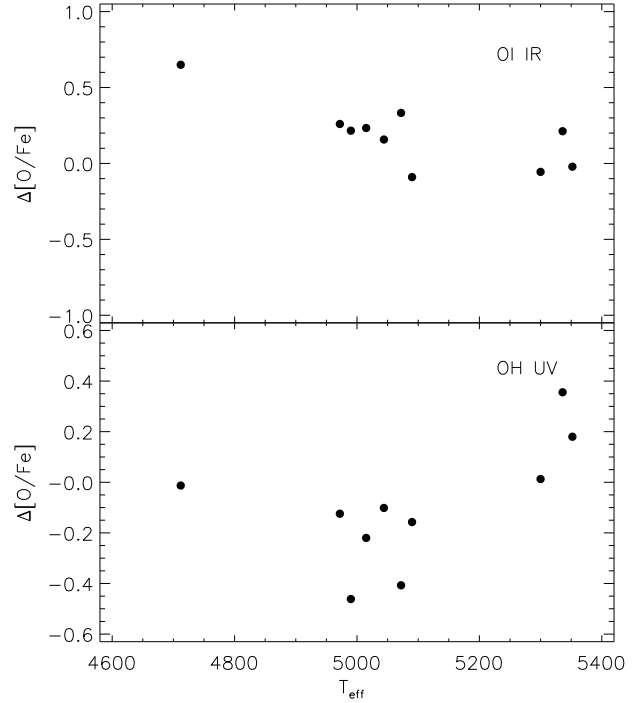


**Fig. 11.** Departures of  $O\text{I}$ -based (top panel) and  $OH$ -based (bottom panel) abundance estimates from  $[O\text{I}]$ -based abundances as a function of  $T_{\text{eff}}$ .

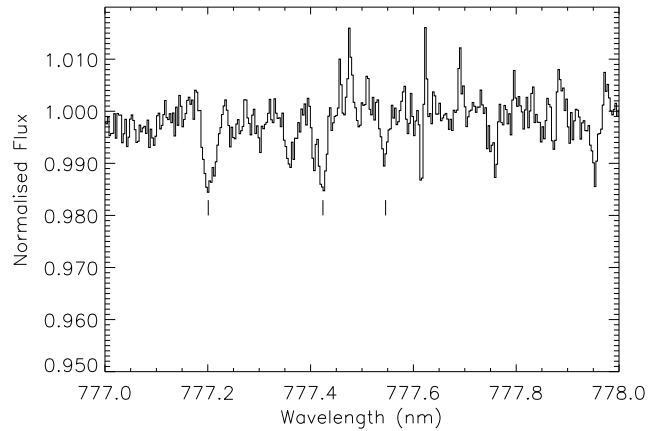


**Fig. 12.** UVES-spectra of HD 126587 around the  $O\text{I}$  IR triplet 777.1-5 nm lines. Vertical bars point out the expected positions of the three lines.

abundance may be required to fit its observed  $OH$  lines. However, the  $[O/Fe]$  values based on the forbidden and permitted lines are also in conflict for this star. In contrast to this star, with the worse agreement between the abundances from the three indicators, there is HD 108317 with the best agreement:  $[O/Fe] = 0.74$  ( $[O\text{I}]$ ), 0.68 ( $O\text{I}$ ) and 0.75 ( $OH$ ).

We have explored whether a change of the  $T_{\text{eff}}$  scale such that an assumed shift of  $T_{\text{eff}}$ , which in turn would also be a function of  $T_{\text{eff}}$ , could provide an explanation for the trend found for the abundance differences. We did not find any obvious such possibility. We noted, however, that the departure of our Hipparcos-based gravity estimates from the isochrone-based estimates depends on the value assumed for  $T_{\text{eff}}$ . The assumed gravity values of the coolest stars are much higher than the values based on isochrones, while the values for the warmest stars are much lower.

### 5.2. Possible systematic errors: NLTE and 3D effects

Up to this point, we have discussed the differences between the oxygen abundances derived from the different abundance criteria in terms of errors in stellar parameters and observations. However we suspect that our 1D-LTE abundance estimates are affected by systematic errors.

The analysis of the oxygen IR triplet lines was carried out with consideration of NLTE effects, and due to this the differences between the results and those of the [O I] line analysis were reduced. The latter is expected to be immune to NLTE effects (Kiselman 1993). The [O/Fe] estimates may still be subject to other systematic errors, e.g. caused by thermal inhomogeneities in the stellar atmospheres. At least for main-sequence stars, the agreement between the forbidden and permitted lines does not seem to improve with the use of 3D hydrodynamical model atmospheres, sooner the opposite seems to occur (Nissen et al. 2002). Abundance corrections for oxygen in the 3D model atmospheres for dwarfs of low metallicities are negative (Nissen et al. 2002) and they tend to be more important for [O/Fe] estimates from [O I] than those from the O I triplet. There are some indications that this may be the case also for subgiants (Nissen et al. 2002; Shchukina et al. 2004). 3D calculations for main-sequence stars also suggest that the 3D [O/Fe] corrections are more significant at low metallicities. From Table 13 one can see that the most-metal poor stars indeed tend to have the greatest discrepancies between the results from the different criteria.

In main-sequence stars the OH lines are more affected by 3D effects than the forbidden line, leading to enhanced OH lines, i.e. smaller abundances. These effects depend mainly on [Fe/H] and to a lesser degree on effective temperature; 3D corrections to [O/Fe] decrease with decreasing effective temperature and increasing metallicity (Asplund & García Pérez 2001). The tendency in the bottom panel of Fig. 11 is consistent with these computations. However, we do not trace any dependence on stellar metallicity although 3D-effects on [O/Fe] from [O I] as well as from OH are both expected to depend on metallicity (Asplund & García Pérez 2001; Nissen et al. 2002).

Schematic NLTE calculations for OH UV lines suggest that departures from LTE line formation occur mainly because the radiation fields and source functions are higher than the local Planck function (Asplund & García Pérez

2001). Therefore, one would expect that NLTE abundance corrections for the lines in Table 10 should be positive (i.e. increase the abundances) and may depend on effective temperature as well as on metallicity. This may be one reason for the discrepancies between results based on these lines and the [O I] line. Typical values for the corrections in dwarfs are of the order of 0.2 dex (Asplund & García Pérez 2001) and there is evidence for a dependency on metallicity: the corrections become smaller as the metallicity increases. However, these results are based on the two-level approach which may be not appropriate for OH lines, thus NLTE effects should be investigated further. A full NLTE treatment is expected to increase the value of [O/Fe] which will compete with the 3D-effects that will decrease [O/Fe].

Once 3D-hydrodynamical model atmospheres are available for subgiants of Pop II, 3D-effects on our [O/Fe] estimates should be investigated.

### 5.3. The galactic evolution of oxygen – comparisons to other studies

We have discussed the discrepancies between the results from the different indicators for the oxygen abundance and suggest that our (1D-LTE) results based on the [O I] 630.03 nm line are to be preferred. We shall now comment on the galactic evolution of oxygen according to these results. In recent years, work done especially based on the forbidden line has suggested a trend in [O/Fe]-vs-[Fe/H] that is flat at low metallicities while several studies based on OH UV electronic transitions (Israelian et al. 1998, 2001; Boesgaard et al. 1999) suggest a linear trend, with [O/Fe] gradually rising to high levels at the lowest metallicities.

Among our results some data points around  $-2.0$  disturb the picture of a possible flat trend in [O/Fe]-vs-[Fe/H] at a level of 0.55 (see top panel in Fig. 10). The scatter in [O/Fe] around that metallicity is barely significant,  $\sim 0.14$  (s.d.). [O/Fe] ranges from 0.41 to 0.74; the values departing most from the mean correspond to HD 4306 and HD 108317. While the last star is among those showing the best agreement among abundances from the three indicators, HD 4306 is one where the indicators disagree severely. HD 27928 and BD-01°2582, with low [O/Fe] values, are confirmed and claimed binaries (Carney et al. 2003), respectively, so their abundances may be contaminated. Note, however, that HD 108317 may be a binary, according to Carney et al. (2003). HD 128279 has a low [O/Fe] value, but is another star with poor agreement among the indicators. On the other hand, a linear fit to the data points in the top panel of Fig. 10 is difficult to establish, especially due to the scatter at low metallicity. We note that our result for the metal-poor giant HD 126587, with its relatively low [O/Fe] ( $\sim 0.45$ ), has a great effect on attempts to judge whether there is a "flat" tendency or a gradual increase in [O/Fe] when proceeding towards low metallicities. The result of a linear fit to the data

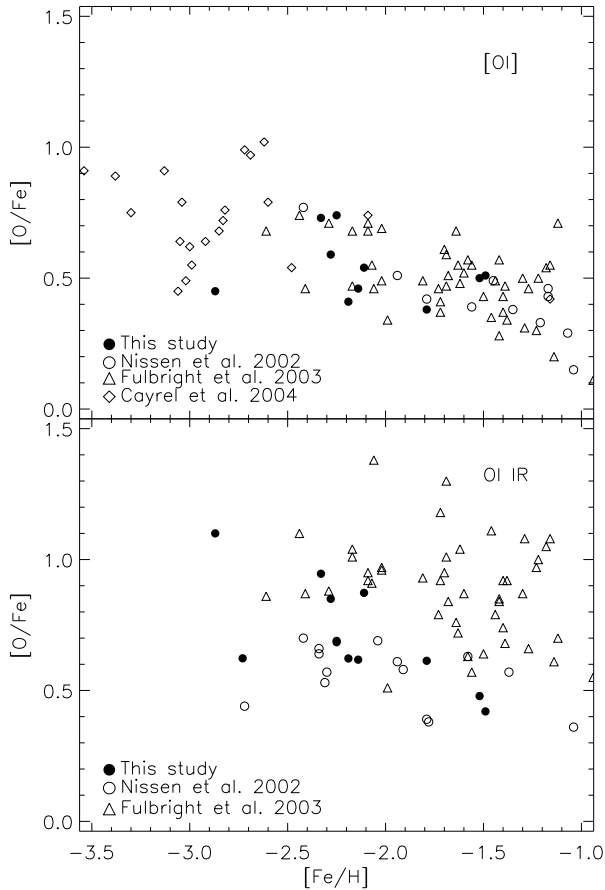


**Fig. 13.** Comparison of  $[O/Fe]$  values in Table 13 with results from: Nissen et al. (2002), Fulbright & Johnson (2003) and Cayrel et al. (2004). Results based on the  $[O I]$  line are shown in the top panel while results based on the O I triplet are shown in the bottom panel. A consistent value for the solar oxygen abundance, 8.74 dex, was adopted for all the data points.

points is  $[O/Fe] = -0.09(\pm 0.08)[Fe/H] + 0.36(\pm 0.15)$ . If instead, metallicities based on the Fe I are assumed, this trend becomes steeper. This is due to the dependence on metallicity of the iron abundance differences discussed in Sect. 3.6.

We have chosen to compare our results with four studies in which the metallicity ranges overlap with ours: Israelian et al. (1998); Nissen et al. (2002); Fulbright & Johnson (2003); Cayrel et al. (2004). The results in Nissen et al. (2002) are easy to compare with because we have used the same method and the same tools. The methods used by Fulbright & Johnson (2003) and Cayrel et al. (2004) are also very similar to ours although the tools are partly different. The method utilised by Israelian et al. (1998) is somewhat deviating from ours. No attempt was made to homogenize the scales of stellar parameters in the comparison with them. In the Fulbright & Johnson (2003) case, we could use the option

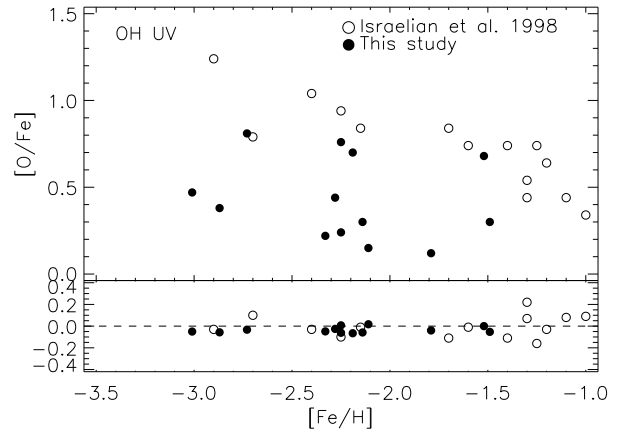


**Fig. 14.** Comparison between our results and those of Israelian et al. (1998) as regards  $[O/Fe]$  values based on the OH line at 316.7 nm. The bottom panel shows how the  $[O/Fe]$  values based on the single OH line at 316.7 nm deviate from the mean values for all OH lines used in the study. The same solar oxygen abundance, 8.74, was used for all data points.

to compare to abundance results based on the Alonso et al. temperature scale.  $[O/Fe]$  values plotted in Fig. 13 were calculated from the values of  $[Fe/H]$  and  $\log \epsilon_O$  as reported in the different papers after corrections of oxygen abundances for differences in the assumed  $\log gf$ -values. For the solar oxygen abundance, we took 8.74 dex, see Sect. 4.1.

The different studies cover different stellar evolutionary phases. While Israelian et al. (1998) and Nissen et al. (2002) mainly study main-sequence stars, Fulbright & Johnson (2003) and Cayrel et al. (2004) analyse subgiants or giants. Our study goes to lower metallicities than the studies of Nissen et al. and Fulbright et al. but not as low as Cayrel et al. (Fig. 13). In general, our  $[O/Fe]$  values, whether based on the forbidden or the triplet lines, follow the same tendencies with  $[Fe/H]$  as in the other studies. For oxygen abundances from the forbidden line, see top panel in Fig. 13, there is no clear distinction between our and the rest of the data points. For the triplet line results (bottom panel) there is a systematic difference between, on one hand our results and those of Nissen et al., relative to those of Fulbright et al. on the other; a differentiation which seems to occur between dwarfs and giants. In that plot, most of our subgiants lie close to the dwarfs from Nissen et al., especially the not very cool ones. A few of the cooler stars get instead close in  $[O/Fe]$  to the giants of Fulbright et al.

We have three stars in common with Fulbright & Johnson (2003): HD 45282, HD 108317 and HD 218857. These authors derived oxygen abundances from both the permitted and the forbidden oxygen lines using two different stellar parameter scales. We have compared our results with their results for the Alonso et al. scale with consideration of the differences

in the assumed stellar parameters, and find that our and their abundances agree to within 0.1 dex. We note that they use Kurucz model atmospheres and that their oxygen abundance estimates are based on the use of both forbidden lines.

In order to compare our results from OH with the linear fit suggested by Israelian et al. (1998), it is necessary to displace their fit by 0.2 dex along the vertical axis to account for the difference in the adopted solar oxygen abundance. Our results lie below theirs. This could be due to the use of a different set of OH UV lines or due to the use of different oscillator strength values. These possibilities have been explored by a comparison based on the only OH line in common (316.7 nm). The oxygen abundances were corrected for the differences in the  $\log gf$ -value ( $-1.694$  versus  $-1.544$ ), and plotted in Fig. 14. Obviously, our data points lie significantly below those of Israelian et al.; only the subgiants with the highest  $T_{\text{eff}}$  may be close. We remind the reader that the effective temperature for two of these stars (HD 45282 and HD 128279) may have been overestimated and that if a decrease of 100 K in their temperatures (see Sect. 3.6) is taken into account the data points corresponding to these stars will move down in the figure and consequently away from the ones of Israelian et al. However, the decrease in gravity suggested for other two stars of our sample (HD 4306 and CD-24° 1782) in Sect. 3.6 would instead move up these two objects. In conclusion, although star-to-star differences may change if the above mentioned changes in  $T_{\text{eff}}$  and  $\log g$  respectively are applied, the mean difference between our abundances and Israelian et al. is almost unaffected.

The bottom panel in Fig. 14 shows how the  $[\text{O}/\text{Fe}]$  values based on the single line depart from the mean values for all OH lines used in each study. These departures are quite small compared with the differences between us and Israelian et al. Those differences are probably due to the fact that Israelian et al. analysed stars close to the turn-off point. These stars are expected to show greater effects due to thermal inhomogeneities on the abundances derived from OH lines than our cooler subgiants (Asplund & García Pérez 2001; Nissen et al. 2002).

In general, the systematic differences in oxygen abundances between dwarfs and giants found in the present study may most probably be explained as results of a change with effective temperature and surface gravity of the systematic errors, as was already suggested by line computations for OH UV lines in 3D model atmospheres by Asplund & García Pérez (2001).

## 6. Conclusions

Until 3D hydrodynamic model atmospheres for subgiants are available which will make 3D-NLTE line formation computations possible, 1D-LTE analyses based on the forbidden 630.03 nm line of oxygen will probably provide the best estimates of stellar  $[\text{O}/\text{Fe}]$  when observable. These values are by far the most accurate, with typical errors of the order of 0.10 dex. Note although that

they may not be free of significant systematic errors associated with inhomogeneities in the stellar atmospheres. Our best  $[\text{O}/\text{Fe}]$  estimates suggest a value at a level of  $0.55 \pm 0.13$  for Pop II subgiants, relatively independent on metallicity; the best linear fit to these estimates is  $[\text{O}/\text{Fe}] = -0.09(\pm 0.08)[\text{Fe}/\text{H}] + 0.36(\pm 0.15)$ .

Both  $[\text{O}/\text{Fe}]$  values based on the IR triplet lines and on the OH UV lines depart from the the  $[\text{O I}]$ -based estimates. The departures from the  $[\text{O I}]$  results are more significant for the abundances derived from the triplet lines, on average  $0.19 \pm 0.22$  dex (s.d.), than for the values from the molecular lines,  $-0.09 \pm 0.25$  dex (s.d.). In the case of the triplet lines, the departures decrease with increasing effective temperatures while in the case of the OH lines they increase, turning from being negative to positive. According to line computations for 3D model atmospheres of main-sequence stars, 3D abundance corrections are negative and decrease with decreasing effective temperature which is not in contradiction with the present observations. In general, 3D effects on abundances and departures from LTE depend on stellar parameters and this can be the reason for the fact that differences in  $[\text{O}/\text{Fe}]$  between the indicators depend on the fundamental stellar parameters.

In order to increase the accuracies of  $[\text{O}/\text{Fe}]$  the  $S/N$  in the observations should be further improved and the effective temperatures should be determined more accurately. Accurate gravities are as well necessary to improve the values based on OH UV lines whose typical errors are of the order of 0.3 dex.

Our results for subgiants follow the trends found by many others for main-sequence stars and giants in the last few years with the exception of our OH-based results which are significantly lower.

*Acknowledgements.* We thank A. Goldman for providing us with the  $\log gf$  values for OH lines. We are grateful to K. Eriksson and N. Piskunov for fruitful discussions. An important part of this work was carried out during the visit of the first author to ESO and she much appreciate their hospitality and financial support. The work had been supported by the Nordic Optical Telescope and the Swedish Research Council. This publication makes use of data products from the Two Micron All Sky Survey, which is a joint project of the University of Massachusetts and the Infrared Processing and Analysis Center/California Institute of Technology, funded by the National Aeronautics and Space Administration and the National Science Foundation.

## References

- Abia, C. & Rebolo, R. 1989, ApJ, 347, 186
- Allende Prieto, C., Lambert, D. L., & Asplund, M. 2001, ApJL, 556, L63
- Alonso, A., Arribas, S., & Martínez-Roger, C. 1999, A&AS, 140, 261
- Anders, E. & Grevesse, N. 1989, Geochimica et Cosmochimica Acta, 53, 197
- Asplund, M. 2005, ARA&A, 481

- Asplund, M. & García Pérez, A. E. 2001, *A&A*, 372, 601
- Asplund, M., Grevesse, N., Sauval, A. J., Allende Prieto, C., & Kiselman, D. 2004, *A&A*, 417, 751
- Asplund, M., Gustafsson, B., Kiselman, D., & Eriksson, K. 1997, *A&A*, 318, 521
- Asplund, M., Nordlund, Å., Trampedach, R., & Stein, R. F. 1999, *A&A*, 346, L17
- Asplund, M., Nordlund, Å., Trampedach, R., & Stein, R. F. 2000, *A&A*, 359, 743
- Balachandran, S. C. & Bell, R. A. 1998, *Nat*, 392, 791
- Balachandran, S. C., Carr, J. S., & Carney, B. W. 2001, *New Astronomy Review*, 45, 529
- Barbuy, B. 1988, *A&A*, 191, 121
- Barbuy, B., Meléndez, J., Spite, M., et al. 2003, *ApJ*, 588, 1072
- Barklem, P. S., Stempels, H. C., Allende Prieto, C., et al. 2002, *A&A*, 385, 951
- Bell, R. A., Balachandran, S. C., & Bautista, M. 2001, *ApJL*, 546, L65
- Bergbusch, P. A. & Vandenberg, D. A. 2001, *ApJ*, 556, 322
- Bessell, M. S., Castelli, F., & Plez, B. 1998, *A&A*, 333, 231
- Bessell, M. S., Hughes, S. M. G., & Cottrell, P. L. 1984, *Proceedings of the Astronomical Society of Australia*, 5, 547
- Bessell, M. S., Sutherland, R. S., & Ruan, K. 1991, *ApJL*, 383, L71
- Biemont, E., Baudoux, M., Kurucz, R. L., Ansbacher, W., & Pinnington, E. H. 1991, *A&A*, 249, 539
- Boesgaard, A. M., King, J. R., Deliyannis, C. P., & Vogt, S. S. 1999, *AJ*, 117, 492
- Carlsson, M. 1986, *Uppsala Astronomical Observatory Report No. 33*
- Carney, B. W., Latham, D. W., Stefanik, R. P., Laird, J. B., & Morse, J. A. 2003, *AJ*, 125, 293
- Carretta, E., Gratton, R. G., & Sneden, C. 2000, *A&A*, 356, 238
- Cayrel, R., Andersen, J., Barbuy, B., et al. 2001, *New Astronomy Review*, 45, 533
- Cayrel, R., Depagne, E., Spite, M., et al. 2004, *A&A*, 416, 1117
- Collet, R., Asplund, M., & Thévenin, F. 2005, *A&A*, in press
- Conti, P. S., Greenstein, J. L., Spinrad, H., Wallerstein, G., & Vardya, M. S. 1967, *ApJ*, 148, 105
- Cunto, W., Mendoza, C., Ochsenbein, F., & Zeippen, C. J. 1993, *A&A*, 275, L5+
- Dekker, H., D'Odorico, S., Kaufer, A., Delabre, B., & Kotzlowski, H. 2000, in *Proc. SPIE Vol. 4008*, p. 534-545, *Optical and IR Telescope Instrumentation and Detectors*, Masanori Iye; Alan F. Moorwood; Eds., 534-545
- Fuhrmann, K., Axer, M., & Gehren, T. 1993, *A&A*, 271, 451
- Fulbright, J. P. & Johnson, J. A. 2003, *ApJ*, 595, 1154
- Fulbright, J. P. & Kraft, R. P. 1999, *AJ*, 118, 527
- Gillis, J. R., Goldman, A., Stark, G., & Rinsland, C. P. 2001, *Journal of Quantitative Spectroscopy and Radiative Transfer*, 68, 225
- Gratton, R. G., Carretta, E., Eriksson, K., & Gustafsson, B. 1999, *A&A*, 350, 955
- Grevesse, N. & Sauval, A. J. 1998, *Space Sci. Rev.*, 85, 161
- Gustafsson, B., Bell, R. A., Eriksson, K., & Nordlund, A. 1975, *A&A*, 42, 407
- Hakkila, J., Myers, J. M., Stidham, B. J., & Hartmann, D. H. 1997, *AJ*, 114, 2043
- Hinkle, K. H. & Lambert, D. L. 1975, *MNRAS*, 170, 447
- Israelian, G., García López, R. J., & Rebolo, R. 1998, *ApJ*, 507, 805
- Israelian, G., Rebolo, R., García López, R. J., et al. 2001, *ApJ*, 551, 833
- Kiselman, D. 1993, *A&A*, 275, 269
- Kiselman, D. 2001, *New Astronomy Review*, 45, 559
- Kiselman, D. & Nordlund, A. 1995, *A&A*, 302, 578
- Korn, A. J., Shi, J., & Gehren, T. 2003, *A&A*, 407, 691
- Kurucz, R. 1993, *Diatomic Molecular Data for Opacity Calculations*. Kurucz CD-ROM No. 15. Cambridge, Mass.: Smithsonian Astrophysical Observatory, 1993., 15
- Kurucz, R. L., Furenlid, I., & Brault, J. 1984, *Solar flux atlas from 296 to 1300 NM (National Solar Observatory Atlas, Sunspot, New Mexico: National Solar Observatory, 1984)*
- Meléndez, J., Barbuy, B., & Spite, F. 2001, *ApJ*, 556, 858
- Munari, U. & Zwitter, T. 1997, *A&A*, 318, 269
- Nissen, P. E., Gustafsson, B., Edvardsson, B., & Gilmore, G. 1994, *A&A*, 285, 440
- Nissen, P. E., Hoeg, E., & Schuster, W. J. 1997, in *ESA SP-402: Hipparcos - Venice '97*, 225-230
- Nissen, P. E., Primas, F., Asplund, M., & Lambert, D. L. 2002, *A&A*, 390, 235
- O'Brian, T. R., Wickliffe, M. E., Lawler, J. E., Whaling, J. W., & Brault, W. 1991, *Optical Society of America Journal B Optical Physics*, 8, 1185
- Piskunov, N. E., Kupka, F., Ryabchikova, T. A., Weiss, W. W., & Jeffery, C. S. 1995, *A&AS*, 112, 525
- Przybilla, N. & Butler, K. 2004, *ApJ*, 609, 1181
- Schlegel, D. J., Finkbeiner, D. P., & Davis, M. 1998, *ApJ*, 500, 525
- Schuster, W. J. & Nissen, P. E. 1988, *A&AS*, 73, 225
- Shchukina, N., Bueno, J. T., & Asplund, M. 2004, *ArXiv Astrophysics e-prints*
- Sneden, C., Kraft, R. P., Prosser, C. F., & Langer, G. E. 1991, *AJ*, 102, 2001
- Thévenin, F. & Idiart, T. P. 1999, *ApJ*, 521, 753
- Tinsley, B. M. 1980, *A&A*, 89, 246
- Vandenberg, D. A., Swenson, F. J., Rogers, F. J., Iglesias, C. A., & Alexander, D. R. 2000, *ApJ*, 532, 430
- Wheeler, J. C., Sneden, C., & Truran, J. W. 1989, *ARA&A*, 27, 279
- Wiese, W. L., Fuhr, J. R., & Deters, T. M. 1996, *Atomic transition probabilities of carbon, nitrogen, and oxygen : a critical data compilation (Edited by W.L. Wiese, J.R. Fuhr, and T.M. Deters. Washington, DC :*



American Chemical Society ... for the National Institute  
of Standards and Technology (NIST) c1996. QC 453  
.W53 1996.)